THE ASTROPHYSICAL JOURNAL, 297:766–786, 1985 October 15

THE NEUTRAL-GAS DISK AROUND THE GALACTIC CENTER

R. GENZEL,[1] DAN M. WATSON,[2] M. K. CRAWFORD,[1] AND C. H. TOWNES[1]

Received 1984 December 26; accepted 1985 April 22

ABSTRACT

Detailed far-infrared observations of several atomic and ionic fine-structure lines and molecular rotational lines toward the Galactic center are discussed. There is an extensive ($\gtrsim 5$ pc radius) neutral gas and dust disk of mass $\gtrsim 10^4\ M_\odot$ surrounding the inner, ionized 2 pc of the Galaxy. This disk is seen almost edge-on and is tilted $\sim 20°$ relative to the Galactic plane. Some ionized gas clouds in the Sgr A West "spiral" are at the inner edge of the neutral disk ($R \sim 1.7$ pc), where it is exposed to Lyman continuum radiation from the center. The bright C^+ and O^0 far-infrared lines and the far-infrared continuum radiation predominantly arise in a photodissociation region between the inner edge of the disk and cooler molecular gas at $R \gtrsim 4$ pc. This photodissociation region is excited by the intense UV radiation from the Galactic center. Some [O I] emission probably comes from neutral cores of ionized gas clouds within the inner cavity. The neutral gas in the Galactic center photodissociation region has a hydrogen density of $\sim 10^5$ cm^{-3} and gas temperature ~ 300 K, and is very clumpy. Volume emissivity and gas density of the warm atomic gas decrease with increasing distance from the center.

We also report the detection of rotational emission lines of highly excited CO and OH molecules and absorption lines from cool OH. The CO emission may come from the photodissociation region if a substantial CO column density ($\gtrsim 10^{18}$ cm^{-2}) and abundance ($[CO]/[H_2] \gtrsim 5 \times 10^{-5}$) exist there. Perhaps more likely, the far-infrared CO emission may come from a smaller column density of hotter gas excited by shock waves. The OH rotational emission may be excited collisionally or by infrared pumping. In either case, a high abundance of OH ($[OH]/[H_2] \sim 10^{-7}$–10^{-5}) is required.

The dominant motion of the neutral gas disk is rotation about an axis similar to the rotation axis of the Galaxy. The rotation velocity at a radius of 2 pc, corrected for inclination, corresponds to an enclosed mass of $(4.8 \pm 1) \times 10^6\ M_\odot$. If the inner, high-velocity [Ne II] clouds observed by Lacy *et al.* (1980) are also in predominantly circular motion, a large fraction of this mass must be contained within 0.2 pc of the center, and the mass distribution is more condensed than that of an isothermal stellar cluster. If the ionized clouds have fallen into the center from the neutral disk, however, no strong central condensation is required. There are also noncircular motions which may be accounted for by a combination of cloud-cloud turbulence, by [O I] emission from the central 2 pc, and by noncircular, resonant orbits in a slightly barred gravitational potential.

Subject headings: galaxies: Milky Way — galaxies: nuclei — infrared: sources — infrared: spectra — interstellar: abundances — interstellar: molecules

I. INTRODUCTION

Observations of the far-infrared emission from warm dust (Becklin, Gatley, and Werner 1982, hereafter BGW) and of the 63 μm $^3P_1 \rightarrow {}^3P_2$ fine-structure line of neutral atomic oxygen (Lester *et al.* 1981; Genzel *et al.* 1984, hereafter Paper I) have revealed the presence of a neutral gas cloud directly associated with the Galactic center (Sgr A West) and surrounding the central ionized region (cf. Lacy *et al.* 1980; Lacy, Townes, and Hollenbach 1982; see also the review by Brown and Liszt 1984). These earlier observations have shown the following:

1. The far-infrared continuum and [O I] line sources are extended over about 10 pc (3′) approximately along the Galactic plane and are centered on the radio source Sgr A West. The dust continuum emission at $\lambda \geq 50$ μm is double-lobed, with emission peaks 30″ in longitude to either side of the compact infrared source IRS 16.

2. The dust temperature decreases with radius, and there is much less dust density at $R \leq 1.5$ pc than at $R \geq 1.5$ pc. The heating of dust and gas in the neutral "lobes" is most likely due to UV radiation from the center. Because of the lack of material in the inner 1.5 pc, much of the $\sim 10^7\ L_\odot$ of UV luminosity escapes to radii greater than 1.5 pc.

3. The [O I]–emitting gas has a temperature $\gtrsim 100$ K, and hydrogen densities are between 10^3 and 10^6 cm^{-3}.

4. The [O I] line-center velocities show that the neutral cloud is rotating around the center. The rotation velocities at $R \sim 1$ pc correspond to an enclosed mass of (2–5) $\times 10^6$ $M_\odot$.

We present here a more detailed investigation of several far-infrared emission lines arising from this region. The new observations give better and more quantitative information on the physical state and energy balance of the neutral gas, on the motions of the gas as a probe of the mass distribution, and on the relationship between the warm, neutral gas and the ionized gas in the central 1 pc as well as cooler, molecular clouds at $R \gtrsim 5$ pc.

II. OBSERVATIONS

The data were taken with the 91.4 cm telescope on board the NASA Kuiper Airborne Observatory in two flight series to and from Hickam Field (Honolulu, Hawaii) in 1981 June and 1982 July and in several flights from Richmond Royal Air Force Base (Sydney, Australia) in 1983 May. The spectrometer was the University of California, Berkeley, tandem Fabry-Perot

[1] Department of Physics, University of California, Berkeley.
[2] Department of Physics, California Institute of Technology.

described by Storey, Watson, and Townes (1980) and Watson (1980), with photoconductive detectors. The system noise-equivalent power (NEP), including all atmospheric and instrumental losses, was between 7×10^{-15} and 15×10^{-15} W Hz$^{-1/2}$ between 145 and 163 μm, 2×10^{-14} W Hz$^{-1/2}$ at 119 μm, and 6×10^{-14} W Hz$^{-1/2}$ at 63 μm. Table 1 is a list of the line rest wavelengths, observing dates, FWHM velocity resolutions, beam sizes, and continuum flux densities used for absolute calibration (accuracy $\pm 30\%$) at each wavelength. Relative wavelength calibrations were established by measuring interference fringes of a He-Ne laser at 0.6328 μm reflected from the scanning Fabry-Perot metal mesh mirrors. Velocities are accurate to 5–20 km s^{-1}, depending on spectral resolution and signal-to-noise ratio. Chopper throws were between 4′ and 6′ in azimuth, that is, from 60° to 120° relative to the Galactic plane.

The relative pointing and tracking accuracy for a typical 5–10 minute integration at one position was $\pm 5''$. Judging from the good agreement between the 63 μm dust continuum map obtained simultaneously with the 30″ [O I] line data and the continuum map by BGW, we well as from the symmetry of the [O I] velocities along Galactic longitude, we estimate that the nominal zero position ($\Delta l = 0$, $\Delta b = 0$ in all maps and spectra) is at right ascention $17^h42^m28^s.7$, declination $-28°59'14''$ (1950) with an overall accuracy of 10″. This position is offset by 10″ toward positive Galactic latitude from IRS 16 and the radio point source (cf. Brown, Johnston, and Lo 1981; Ekers *et al.* 1983; Storey and Allen 1983). The nominal zero position of the 146 μm [O I] and 163 μm CO and OH measurements also was within 15″ of that position. The pointing during the 158 μm [C II] observations was apparently shifted by $\Delta l = +20''$ relative to the nominal position, and the observations were corrected to the same coordinate system as in the other observations. In what follows, we assume that the distance to the Galactic center is 10 kpc, so that 20″ = 1 pc.

III. RESULTS

Figures 1–4 show the spectral data. In Figure 1 we display spectra of the $^3P_1 \rightarrow {}^3P_2$ fine-structure line of [O I] at 63 μm, taken with 30″ (FWHM) spatial and 100 km s^{-1} (FWHM) spectral resolution. In addition to the spectra shown in Figure 1, [O I] spectra were measured at 10 other positions with 44″ and 200 km s^{-1} resolution to define the [O I] distribution and kinematics over a larger area. The analysis presented here also includes the [O I] data reported earlier (Paper I, resolution 44″ and 150 km s^{-1}). To compare all these measurements quantitatively, we calibrated on spectra taken at or near the (Δl, Δb) = (0, 0) position.

In Figure 2 we show spectra of the upper fine-structure line ($^3P_0 \rightarrow {}^3P_1$) of [O I] at 146 μm, taken with 60″ (FWHM) spatial resolution and 160 km s^{-1} spectral resolution, at positions spaced by 40″ along the Galactic plane at $\Delta b = 0$. In Figure 3 we display spectra of the $^2P_{3/2} \rightarrow {}^2P_{1/2}$ fine-structure line of C^+ at 158 μm, taken with 60″ (FWHM) spatial resolution and 100 km s^{-1} spectral resolution, at several positions along the Galactic plane at $\Delta b = -10''$.

Figure 4*a* is a spectrum at 163 μm taken at $\Delta l = -40''$, $\Delta b = 0$ containing the $J = 16 \rightarrow 15$ rotational line of CO and the two $J = 3/2 \rightarrow 1/2$ rotational transitions of OH in the $^2\Pi_{1/2}$ electronic state. The $J = 3/2$ level is the first state excited in the $^2\Pi_{1/2}$ ladder. In Figure 4*b* are spectra of the 119 μm $^2\Pi_{3/2}$, $J = 3/2 \rightarrow 5/2$ transitions of OH in absorption toward the continuum peaks in Sgr B2 and Sgr A West. These transitions connect the ground state with the first excited rotational state (see also the original detection toward Sgr B2 by Storey, Watson, and Townes 1981).

a) Spatial Distribution of the Atomic Gas

A map of the [O I] 63 μm integrated intensity is presented in Figure 5, superposed on the 15 GHz continuum map of the Sgr A West free-free emission made by Ekers *et al.* (1983) (*left*) and the 63 μm dust continuum emission (*right*). To indicate the connection with the larger scale structures, Figure 6 is the same [O I] map, but superposed on a schematic sketch of a lower resolution 5 GHz radio continuum map by Ekers *et al.* (1983) and the CO $J = 1 \rightarrow 0$ emission at $80 \leq |v_{LSR}| \leq 130$ km s^{-1} from the paper by Liszt, Burton, and van de Hulst (1984). Finally, Figure 7 shows cross-cuts along the Galactic plane

TABLE 1

SUMMARY OF OBSERVATIONS

Line	Observing Date	Spectral Resolution FWHM (km s^{-1})	Spatial FWHM (arcsec)	Resolution Total Area (sr)	Absolute Calibration[a] (Jy)	References
[O I] $^3P_1 \rightarrow {}^3P_2$: 63.1837 μm	1983 May (Australia)	100 200	30 44	2.7×10^{-8} 5.2×10^{-8}	$S_{cont}^{Sgr\ A}$(center) = 3.0×10^3 $S_{cont}^{Sgr\ A} = 6.0 \times 10^3$	1
OH $^2\Pi_{3/2}$, $J = 3/2 \rightarrow 5/2$: $3/2^- \rightarrow 5/2^+$, 119.4410 μm $3/2^+ \rightarrow 5/2^-$, 119.2236 μm	1981 July (Hawaii)	150	44	6×10^{-8}	$S_{cont}^{Sgr\ A} = 2.5 \times 10^3$	2
[O I] $^3P_0 \rightarrow {}^3P_1$: 145.526 μm	1983 May (Australia)	160	60	8×10^{-8}	$S_{cont}^{Sgr\ A} = 1.8 \times 10^3$	3
[C II] $^2P_{3/2} \rightarrow {}^2P_{1/2}$: 157.737 μm	1982 July (Hawaii)	100	60	9×10^{-8}	$S_{cont}^{Sgr\ A} = 1.5 \times 10^3$	4
OH $^2\Pi_{1/2}$, $J = 3/2 \rightarrow 1/2$: $3/2^+ \rightarrow 1/2^-$, 163.1247 μm $3/2^- \rightarrow 1/2^+$, 163.3973 μm	1983 May (Australia)	130	60	1×10^{-7}	$S_{cont}^{Sgr\ A} = 1.4 \times 10^3$	5
CO $J = 16 \rightarrow 15$: 162.8116 μm	1983 May (Australia)	130	60	1×10^{-7}	$S_{cont}^{Sgr\ A} = 1.4 \times 10^3$	6

[a] Calibration on is the line-to-continuum ratio with effective bandwidth $\Delta\nu = \pi/2\Delta\nu_{FWHM}$.

REFERENCES.—(1) Rieke, Telesco, and Harper 1978; Gatley *et al.* 1978; Becklin, Gatley, and Werner 1982. [O I] rest wavelength: Genzel *et al.* 1984; Inguscio *et al.* 1984. (2) OH rest wavelength: Brown *et al.* 1982. (3) Gatley *et al.* 1978. [O I] rest wavelength: Davies *et al.* 1978. (4) Gatley *et al.* 1978. [C II] rest wavelength: Crawford *et al.* 1985. (5) Gatley *et al.* 1978. OH rest wavelength: Brown *et al.* 1982. (6) Gatley *et al.* 1978.

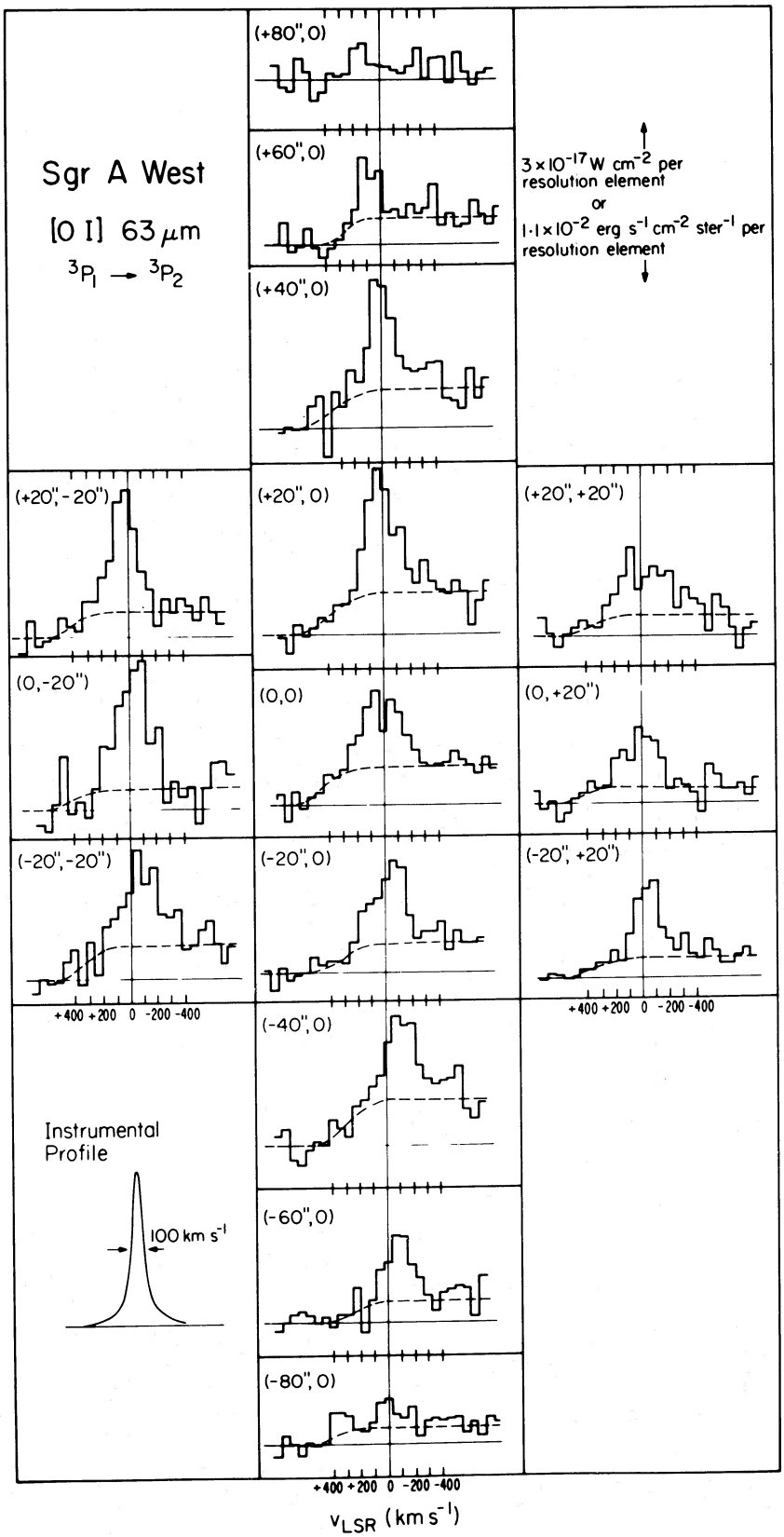

FIG. 1.—Spectra of the $^3P_1 \rightarrow {}^3P_2$ fine-structure line [O I] at 63 μm toward the Galactic center, at FWHM 100 km s^{-1} spectral and 30″ spatial resolution. The Lorentzian instrumental response is shown at lower left. Spectra are displayed as a function of Galactic longitude (*up and down*) and latitude (*left and right*; positive latitude toward the right). The (Δl, Δb) = (0, 0) position is at R.A. = 17^{h}42^{m}28^s.7, decl. = −28°59′14″ (1950). Dashed lines in the spectra indicate the continuum level, with zero intensity marked by a horizontal line. The continuum emission at v_{LSR} = +600 km s^{-1} drops to zero in all spectra because of absorption by telluric H_2O.

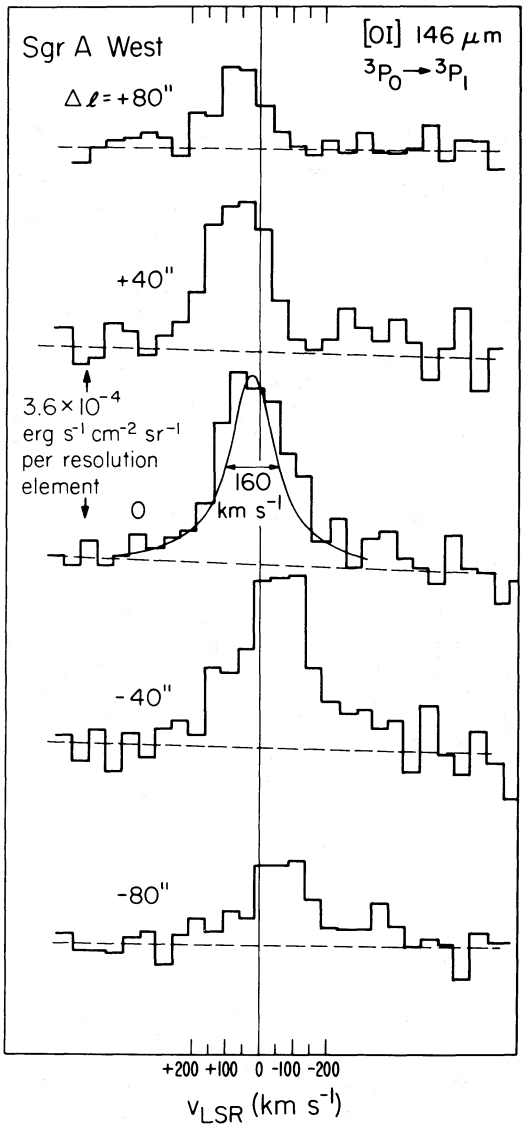

FIG. 2.—Spectra of the $^3P_0 \rightarrow P_1$ fine-structure line of [O I] at 146 μm toward several positions along the Galactic plane. The zero position is the same as in Fig. 1. The FWHM spectral resolution is 160 km s^{-1}, and the spatial resolution is 1′. The intensity scale is given per spectral resolution element.

($\Delta b \sim 0''$) of the [O I] 63 μm data, compared with the other far-infrared lines and the far-infrared continuum emission. The main results of the mapping are described below.

The [O I] source has a FWHM extent of 6 × 4 pc ($\Delta l \times \Delta b$) and is centered on IRS 16 and the radio point source. Significant [O I] emission extends out to a radius of ±5 pc from the center. There are two emission peaks about ±30″ on either side of IRS 16 and approximately in the Galactic plane. The total extent and the double-lobed structure of the [O I] emission are very similar to the distribution of the far-infrared continuum emission; that is, neutral atomic gas and warm dust are coexistent. The [O I] distribution, however, appears not to be identical to the continuum distribution. Compared with the continuum map in Figure 5 (see also BGW; Rieke, Telesco, and Harper 1978), the [O I] peaks appear to be somewhat closer to the nucleus (by about 5″–10″), there may be more [O I] emission at the center position, and the oxygen emission is not as symmetrically placed relative to the Galactic plane. These small differences may be caused by a relatively larger amount of neutral oxygen at $R \lesssim 1$–2 pc compared with dust, or by the sensitivity of the 63 μm line emission to hydrogen density below the critical density of a few times 10^6 cm^{-3}.

Although there is no detailed agreement with the overall spatial distribution of free-free continuum emission, it is now

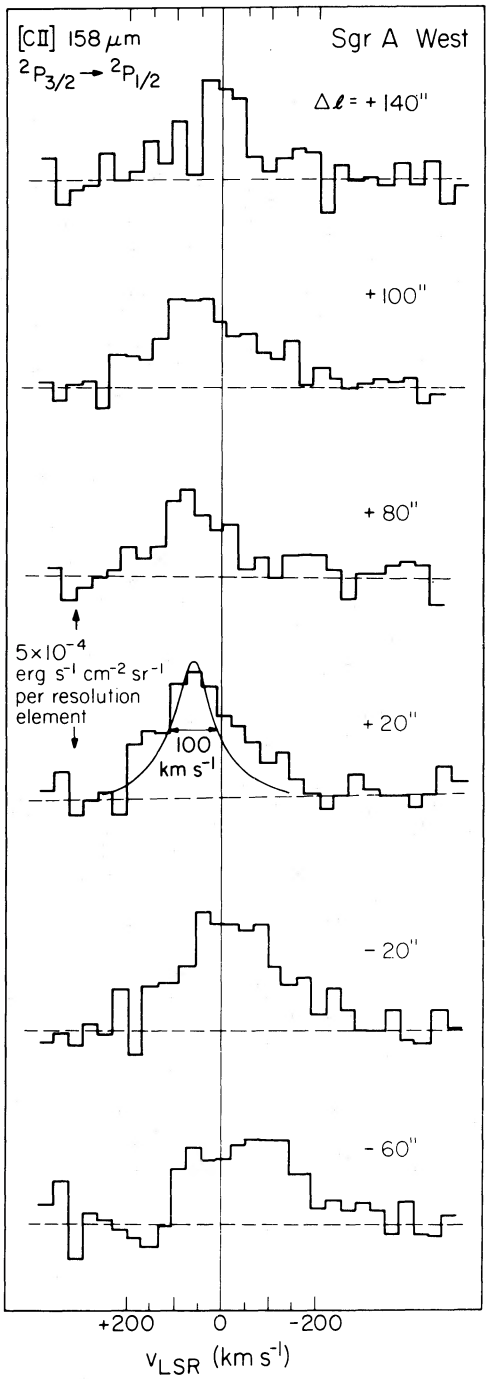

FIG. 3.—Spectra of the $^2P_{3/2} \rightarrow {}^2P_{1/2}$ fine-structure line of [C II] at 158 μm toward spectral positions along the Galactic plane, with FWHM 100 km s^{-1} spectral and 1′ spatial resolution. The zero position is R.A. = 17^{h}42^{m}29^s.3, decl. = −28°59′18″ (1950), which is 10″ toward negative Galactic latitude from the base position in Fig. 1. The intensity scale is given per spectral resolution element.

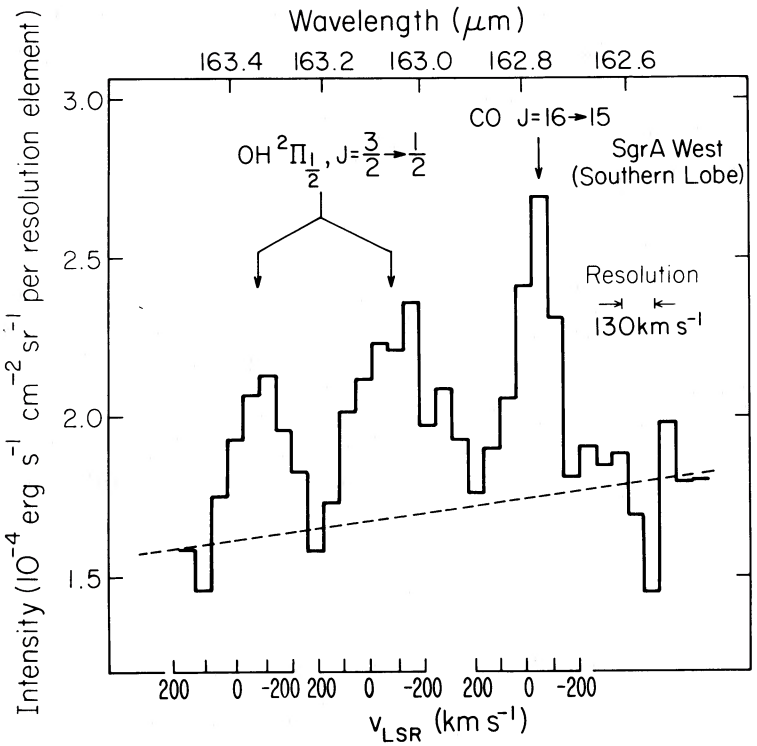

FIG. 4a

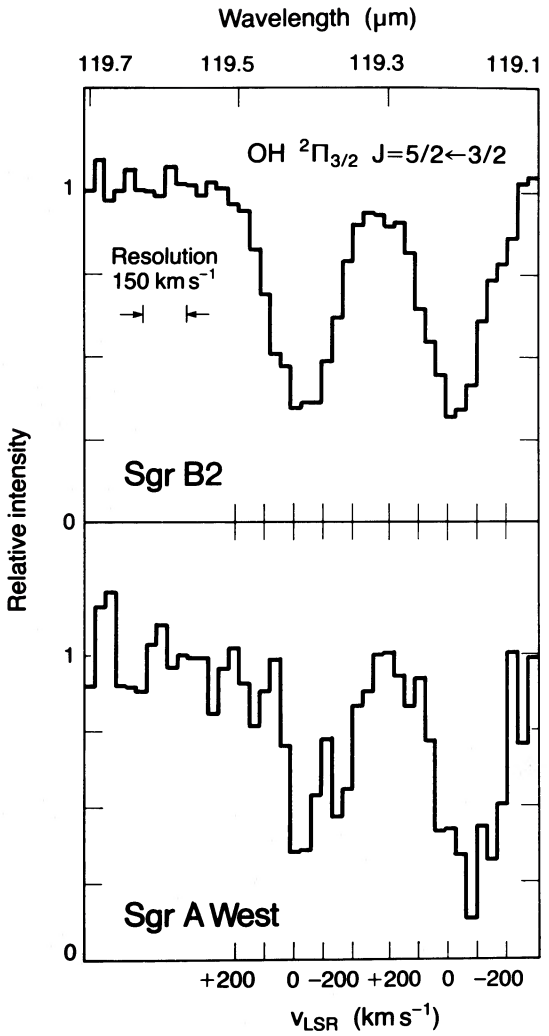

FIG. 4b

FIG. 4.—(*a*) Spectrum of the CO $J = 16 \rightarrow 15$ and the two OH $^2\Pi_{1/2}$, $J = 3/2 \rightarrow 1/2$ rotational transitions at 163 μm toward $(\Delta l, \Delta b) = (-40'', 0)$. The FWHM spectral and spatial resolutions are 130 km s^{-1} and 1′, respectively. (*b*) Spectrum of the OH $^2\Pi_{3/2}$, $J = 3/2 \rightarrow 5/2$ rotational transitions at 119 μm toward the continuum peak in Sgr B2 (*upper panel*) and Sgr A West (*lower panel*). Data are at 45″ spatial and 150 km s^{-1} spectral resolution.

clear that ionized and neutral gas in Sgr A are closely associated. The [O I] source encompasses the free-free emission region, and the [O I] and dust peaks coincide with the endpoints of the ionized filaments on either side of the center. It appears that the largest part of the neutral atomic gas is just outside the inner, ionized cavity (see also the comparison between [O III] and [O I] emission in Fig. 7). The kinematic information presented below strongly supports this picture.

On the larger scale (Fig. 6), the [O I] source appears to be the interface between the Sgr A West H II region and molecular clouds farther out. The 2.6 mm CO $J = 1 \rightarrow 0$ emission at the same velocities as the [O I] emission peaks ±4 pc from the center (Liszt *et al.* 1983; Liszt, Burton, and van de Hulst 1984). This molecular emission probably comes from cooler gas. The geometry of the whole structure is that of a disk, thick ring, or torus, centered on Sgr A West and viewed almost edge-on. The [O I] and dust continuum lobes at $\Delta l = \pm 30''$ represent the inner edge of this ring (cf. BGW). The major axis of the disk appears to be at an angle of about $-20°$ to $-25°$ relative to the Galactic plane, in agreement with the conclusion of Liszt, Burton, and van de Hulst (1984). The distribution of neutral gas on the 1 kpc scale is also tilted relative to the Galactic plane (cf. Burton and Liszt 1978; Liszt and Burton 1980). However, that tilt is about $+20°$ relative to the plane and is, therefore, inclined $\sim 45°$ relative to the inner central gas disk discussed here.

The spatial extent and longitude distribution of the 146 μm [O I] line emission are more or less identical with those of the 63 μm emission, considering the lower spatial resolution and fewer positions observed at 146 μm. The [C II] distribution also is similar, but the data at positive longitudes suggest that the extent of the 158 μm C^+ emission is larger than the [O I] extent.

b) Physical State of the Atomic Gas

Since the far-infrared [O I] and [C II] lines are collisionally excited and their emission is coextensive, their relative intensities can be used to estimate the density and temperature of the emitting region (cf. Watson 1984; Crawford *et al.* 1985). For the present purpose, we take the atomic hydrogen col-

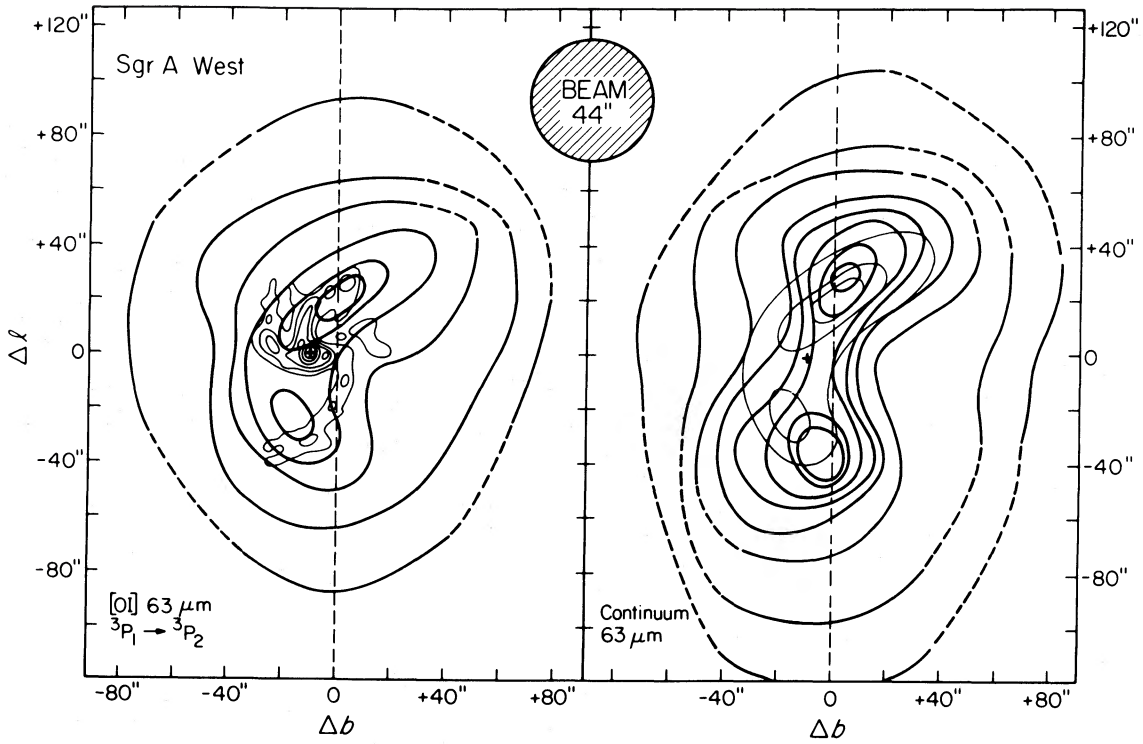

FIG. 5.—(*Left*) Contour maps of integrated 63 μm [O I] flux, as a function of Galactic coordinates, relative to R.A. = $17^h42^m28^s.7$, decl. = 28°59′14″ (1950), superposed on the contours of 2 cm radio continuum free-free emission (the Sgr A West spiral: Ekers *et al.* 1983, 2″ × 3″ resolution). Line contours are in units of 2×10^{-17} W cm^{-2} or 3.6×10^{-3} ergs s^{-1} cm^{-2} sr^{-1}. The radio point source and IRS 16 are at $(\Delta l, \Delta b) \approx (0, -10'')$. Bending upward from the radio point source toward the [O I] peak at $(\Delta l, \Delta b) = (+30'', 0)$ is the northern arm. The radio filament extending from approximately the [O I] peak at $(\Delta l, \Delta b) = (-30'', -10'')$ toward (0, 0) and continuing toward $(+30'', 0)$ is the western arc. The bar feature can be seen as extensions bending from the point source to the left and upward [toward $(+15'', -25'')$] and to the right and upward [toward $(+10'', +15'')$]. (*Right*) Contour map of 63 μm continuum, obtained simultaneously with the line data and superposed on the upper three contours of the [O I] emission. The continuum contours are in units of 10^3 Jy to give a flux of 6000 Jy in a 44″ beam at the center position (extrapolated from BGW and Rieke, Telesco, and Harper 1978). Note that both 30″ and 44″ data were used to make the line and continuum maps of effective FWHM resolution 44″. The maps are well sampled only in the central 80″. Dashed lines show where the contours were interpolated in the outer regions with missing information.

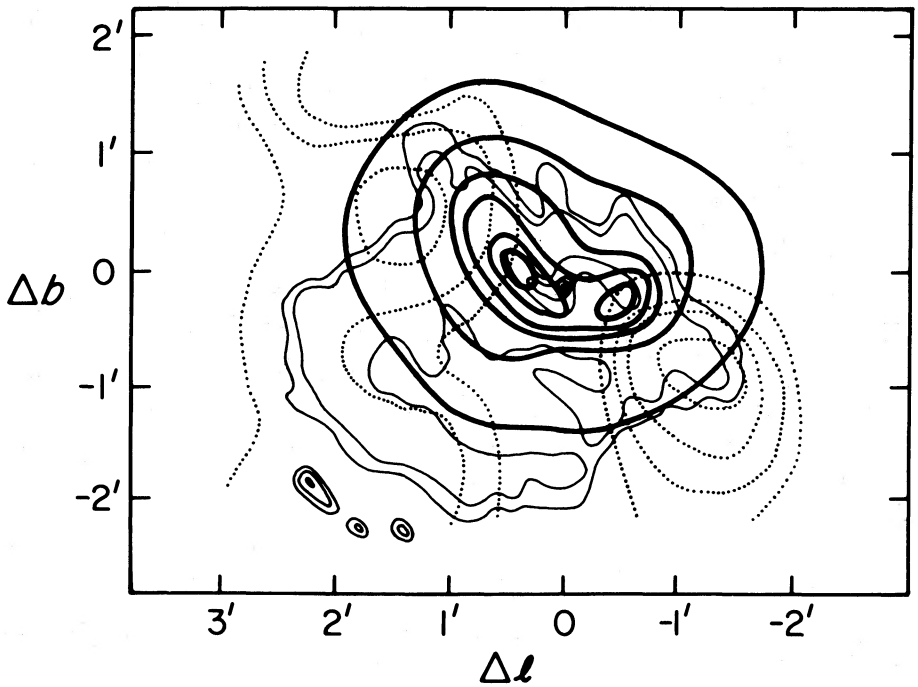

FIG. 6.—Integrated [O I] emission (same data as in Fig. 5), superposed on a schematic sketch of the larger scale radio continuum emission (thin lines: 5 GHz data of Ekers *et al.* 1983, resolution 5″ × 8″) and the CO $J = 1 \rightarrow 0$ clouds at ± 100 km s^{-1} LSR (*dotted curves*: Liszt, Burton, and van de Hulst 1984, resolution 66″). In addition to the "spiral" feature from free-free emission in Sgr A West, there is the nonthermal arc of Sgr A East (at positive Δl and negative Δb), as well as three compact H II regions [near $(\Delta l, \Delta b) = (+2'', -2')$] which are located near the center of the +50 km s^{-1} molecular cloud. The CO data are integrated between $80 \leq |V_{LSR}| \leq 130$ km s^{-1}, and the contours are 210, 240, 270, and 330 K km s^{-1} (radiation temperature times velocity width).

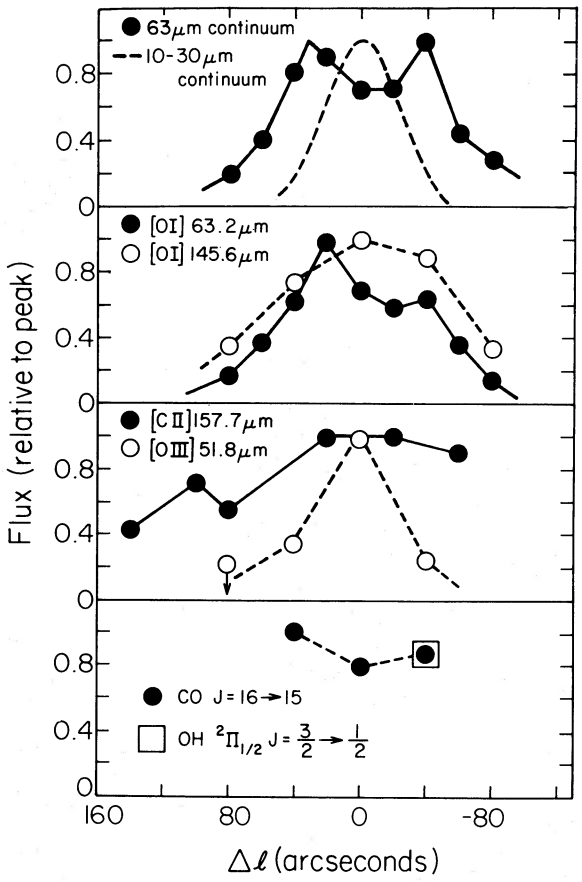

FIG. 7a

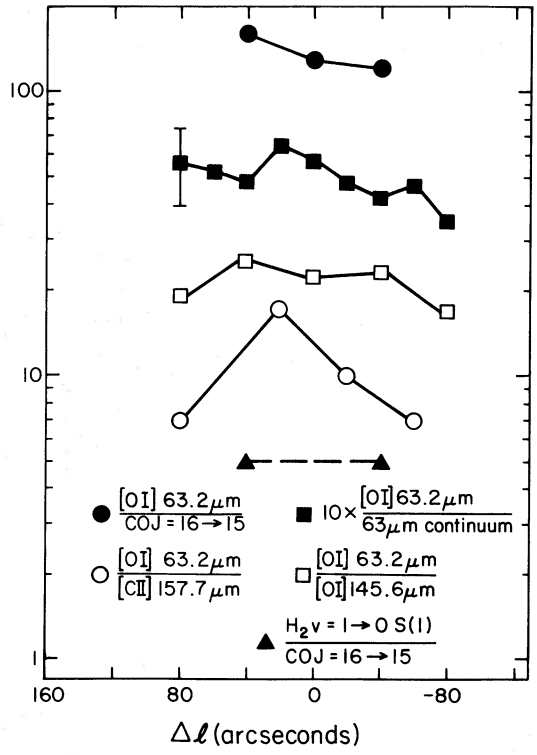

FIG. 7b

FIG. 7.—(*a*) Cross cuts of line and continuum emission along the Galactic plane, relative to the base position of Fig. 5. All line intensities are integrated over profile (*Top panel*) 63 μm continuum emission (*filled circles and thick line*: this paper, 30″ beam, peak flux 4300 Jy) and 30 μm continuum emission (*dashed line*: 30″ beam peak flux 4300 Jy from BGW). (*Second panel from top*) Integrated 63 μm [O I] emission (*filled circles and thick line*: this paper, 30″ beam, peak 6.5×10^{-17} W cm^{-2} or 2.4×10^{-2} ergs s^{-1} cm^{-2} sr^{-1}) and 146 μm [O I] emission (*open circles and dashed line*: this paper, 60″ beam, peak 6.7×10^{-18} W cm^{-2} or 8×10^{-4} ergs s^{-1} cm^{-2} sr^{-1}). (*Third panel from top*) Integrated 158 μm [C II] emission (*filled circle and thick line*: this paper, 60″ beam, peak 1.4×10^{-17} W cm^{-2} or 1.5×10^{-3} ergs s^{-1} cm^{-2} sr^{-1}) and 52 μm [O III] emission (*open circles and dashed line*: Watson *et al.* 1985*a*, 44″ beam, peak 5×10^{-17} W cm^{-2} or 9×10^{-3} ergs s^{-1} cm^{-2} sr^{-1}). (*Bottom panel*) Integrated 163 μm CO $J = 16 \rightarrow 15$ emission (*filled circles and dashed line*: this paper, 60″ beam, peak 1.5×10^{-18} W cm^{-2} or 1.5×10^{-4} ergs s^{-1} cm^{-2} sr^{-1}) and 163 μm OH $^2\Pi_{1/2}$, $J = 3/2 \rightarrow 1/2$ emission (*open rectangle*: this paper, 60″ beam, same peak flux as CO). (*b*) Line/Line and line/continuum ratios as function of longitude offset. The H_2 $S(1)$ flux by Gatley *et al.* (1984) is corrected for 3 mag of 2 μm extinction, and multiplied by a factor of 7 to approximately account for the difference in far-IR and 2 μm beam sizes.

lisional excitation rate coefficients calculated by Launay and Roueff (1977*a*, *b*), and make the assumptions that the emission is optically thin and that the abundance ratio O^0/C^+ is 2.2, the same as the O/C ratio in the solar neighborhood (the results are not very sensitive to the precise value taken for the O^0/C^+ ratio). In Figure 8 we show the calculated loci of constant [O I] 63.2 μm/[C II] 157.7 μm and [O I] 63.2 μm/[O I] 145.6 μm integrated intensity ratio as functions of density and temperature. Indicated on this figure is the line-ratio combination for the northern [O I] peak ($\Delta l = +20''$) and the measurement uncertainty zone for these ratios. For this peak, the derived hydrogen density is 10^5 cm^3 and the temperature is 350 K, leading to a gas pressure of $n_H T = 3 \times 10^7$ cm^{-3} K (see Table 2). As can easily be shown, these values are consistent with the assumption of small line optical depth, even if the source is very clumpy.

Besides the measurement uncertainties, there are systematic effects which may introduce additional uncertainty in the derived density and temperature. For example, a lower O^0/C^+ ratio, or significant optical depth in the [O I] 63.2 μm line, would require high density and temperature. Nevertheless, it seems clear that *the typical hydrogen densities in the neutral ring must be large* ($\sim 10^5$ cm^{-3}) *and that the gas temperature is substantially higher than the dust temperature* (T_{color} = 50–60 K; see BGW). The high neutral gas densities are similar to the typical electron density inferred for the ionized gas in Sgr A West (cf. Lacy *et al.* 1980; Paper I; Lo and Claussen 1983; Serabyn and Lacy 1985; Watson *et al.* 1985*a*).

Determination of variations in density and temperature as a function of position from the data in Figure 7 are somewhat less reliable because of the slightly different beam sizes at the different wavelengths. The general trend can be seen in Figure 7*b*. The ratio of the [O I] 63 μm to [C II] 158 μm line intensities and the ratio of the [O I] 63 μm line to 63 μm continuum intensities decrease on both sides away from the [O I] peak at $\Delta l = +20''$, while the ratio of the two [O I] lines is approximately constant. If this trend is due to radially decreasing excitation of the emission, gas densities in the neutral ring decrease by about a factor of 1.5–2 between 2 and 4.5 pc, while temperatures are approximately constant. The data probably do not exclude the possibility that the line-ratio variations are caused by a combined decrease of density and temperature,

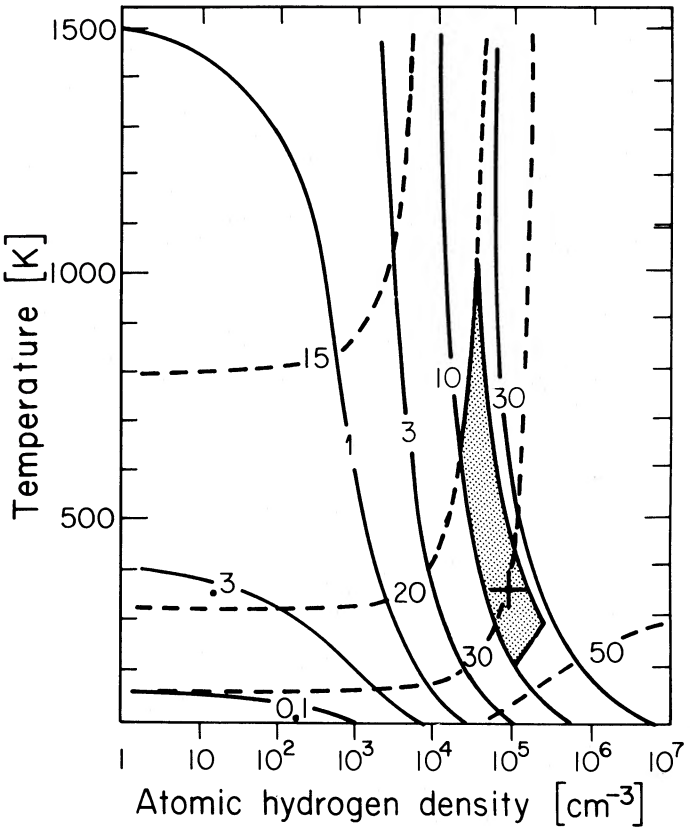

FIG. 8.—Density and temperature of neutral atomic gas in the Galactic center. Solid lines given the loci of constant ratios of [O I] 63 μm/[C II] 158 μm line flux assuming an O^0/C^+ abundance of 2.2. Dashed lines are the loci of constant [O I] 63 μm/[O I] 146 μm line ratios. The cross is the best value of the line ratios toward the northern peak at $(\Delta l, \Delta b) = (+30'', 0)$, and the shaded region gives the 1 σ error zone of this measurement.

since, as can be seen from Figure 8, the [O I]/[C II] ratio at $T \sim 350$ K is more sensitive to temperature than the ratio of the [O I] lines. It is unlikely that the decrease of the [O I]/[C II] ratio is due to an *abundance* effect, since the same UV photons which ionize carbon also contribute significantly to the gas heating.

A strong gradient of the [O I] emissivity as a function of radius from the center is also supported by the 63 μm [O I] intensity distribution itself (Fig. 7*a*). The [O I] emission can be traced to an outer radius of at least $R_o \sim 100''$, but the [O I] brightness distribution is heavily weighted toward the material at $R_i \sim 20''$–$40''$. We have constructed a model of an optically thin ring with $R_o/R_i \sim 4$–5 and a radius-dependent volume emissivity, $\epsilon(R) \sim \epsilon_0 R^{-\alpha}$. The best fit to the [O I] data is for $\epsilon(R) \sim R^{-1}$ to R^{-2}. A ring model with constant emissivity and $R_o/R_i \leq 3$ does not fit the observations. The decrease of [O I] emissivity with radius could be well accounted for by the decreasing UV heating, density, and/or temperature of the gas at larger radii from the center, and is consistent with the decreasing ratio of [O I]/[C II] intensities discussed above. The far-infrared continuum emission from dust also shows a decrease with distance from the center (Fig. 7*a*). BGW have shown that the dust emissivity gradient is probably due to radially decreasing dust temperature as a result of decreasing intensity of the UV radiation field.

c) *Abundance of Carbon and Oxygen*

Since densities and temperatures are suffiently high to populate the C^+ doublet according to the statistical weights of the states, the [C II] line intensity gives a direct estimate of C^+ column density: $N_{C^+} = 10^{18}$ cm^{-2} at $\Delta l = +20''$. The dust continuum measurements between 50 and 400 μm may be used to obtain a hydrogen column density (Rieke, Telesco, and Harper 1978; Gatley *et al.* 1978; BGW; Novak *et al.* 1985). The continuum flux densities were converted to optical depths assuming a dust temperature of 50–60 K (BGW). Hydrogen column densities were computed from the conversion factors from far-infrared opacity to visual extinction given by Hildebrand (1983) and Whitcomb *et al.* (1981), and from $N_H/A_V = 1.9 \times 10^{21}$ cm^{-2} mag^{-1} by Bohlin, Savage, and Drake (1978). The derived hydrogen column density toward the [O I] lobes is $N_{HI+2H_2} = (4 \pm 2) \times 10^{22}$ cm^{-2}. The gas-to-dust mass ratio in the Galactic center may differ from the factor of 100 implied by the above relation, and hence the uncertainty in hydrogen column density is probably larger than the quoted error limits. Hydrogen column densities of $\gtrsim 10^{22}$ cm^{-2} are also obtained from the 21 cm data by Liszt *et al.* (1983). With $N_H \sim 4 \times 10^{22}$ cm^{-2}, the ratio of C^+ column density to total column density of hydrogen nuclei is $(3^{+3}_{-1}) \times 10^{-5}$, and the resulting oxygen abundance is $(7^{+6}_{-2}) \times 10^{-5}$. These abundances are significantly lower than the solar neighborhood abundances of carbon (3×10^{-4}) and oxygen (6.7×10^{-4}). The deficiency of C^+ and O^0 may be interpreted as resulting from a drastically higher dust-to-gas ratio, or from depletion of carbon and oxygen onto grains, or from a large molecular abundance in the neutral disk.

d) *Mass and Clumpiness of the Disk*

With $\sim 4 \times 10^{22}$ cm^{-2} as the beam-averaged hydrogen column density, the gas mass in a 60″ beam centered on each of the lobes is $2 \times 10^3 M_\odot$, and $\sim 2 \times 10^4 M_\odot$ of gas is contained within $R \leq 5$ pc (Table 2). The total amount of cooler molecular gas in the disk beyond $R = 5$ pc (Fig. 6; see also Liszt, Burton, and van de Hulst 1984) may range between an amount equivalent to that in the photodissociation region (if the $J = 1 \rightarrow 0$ CO line is optically thin and $T_{CO} \sim 100$ K) and an amount about a factor of 1.5–2.5 times larger [$(3$–$5) \times 10^4$ $M_\odot$]. The latter case applies if the $J = 1 \rightarrow 0$ CO line is optically thick and the "standard" conversion from CO flux to H_2 column density is applicable [$N_{H_2} = 4 \times 10^{20} \int T^*_{CO} dv$ (K km s^{-1}), where T^*_{CO} is the corrected antenna temperature: cf. Young and Scoville 1982].

From the beam-averaged column density and a size of $\sim$2–3 pc, the *beam-averaged hydrogen volume density* in the [O I] emission region is $\langle n_H \rangle = (7 \pm 3) \times 10^3$ cm^{-3}. The resulting *volume filling factor* of atomic gas is

$$\Phi_v = \frac{\langle n_H \rangle}{n_H} = 10^{-1.2 \pm 0.4} . \quad (1)$$

The beam *area filling factor* Φ_A of the [O I]/[C II] emission depends on the number of layers of clumps, N, along the line of sight:

$$\Phi_A = \Phi_v^{2/3} N = \Phi_v^{2/3} \left(\frac{R}{d_{cc}} \right) = \Phi_v \left(\frac{R}{R_c} \right) , \quad (2)$$

where R is the radius of the region, d_{cc} is the mean clump-clump separation, and R_c is the mean radius of a clump. For $R \sim d_{cc} \sim 2$ pc (one layer), the beam filling factor of the atomic

TABLE 2

PHYSICAL CONDITIONS IN NEUTRAL-GAS DISK AROUND SAGITTARIUS A WEST

Parameter	Value	Remarks
	Atomic Gas	
Gas pressure	$n_H T$ (cm^{-3} K) $= 10^{7.5\pm0.3}$	gas pressure decreases by about a factor of 2 between 2 and 4 pc
Hydrogen density	n_{H,H_2} (cm^{-3}) $= 10^{5\pm0.3}$	
Gas temperature	T (K) $= 350^{+650}_{-150}$	dust temperature is 50–60 K (BGW)
Hydrogen column density	N_{H+2H_2} (cm^{-2}) $= (4 \pm 2) \times 10^{22}$ cm^{-2}	from measurements of dust, 21 cm H I, and CO $J = 1 \rightarrow 0$
Ionized carbon abundance	$\chi_{C^+} = \frac{N_{C^+}}{N_H} = (3^{+3}_{-1}) \times 10^{-5}$	
Neutral oxygen abundance	$\chi_{O^0} = N_{O^0} N_H = (7^{+6}_{-2}) \times 10^{-5}$	ratio of O^0 to C^+ is assumed to be 2.2
Volume filling factor	$\Phi_v = 0.06^{+0.09}_{-0.03}$	
Area filling factor	$\Phi_A = \Phi_v\left(\frac{R}{R_c}\right) \geq \Phi_v^{2/3} \approx 0.2$	$R \sim 2$ pc source radius R_c is clump radius
Total hydrogen mass in photodissociation region	$M_{C^+} \sim 2 \times 10^4\ (M_\odot)$	integrated over $R \leq 5$ pc
	Molecular Gas	
CO abundance	$\chi_{CO} = \frac{N_{CO}}{N_{H_2}} = 6 \times 10^{-5}\left(\frac{10^5\ \text{cm}^{-3}}{n_{H_2}}\right)^{1.25}\left(\frac{300\ \text{K}}{T}\right)^{3.1}$	assuming optically thin emission, collisional excitation, and $N_{2H_2} = 4 \times 10^{22}$ cm^{-2}
OH abundance	$\chi_{OH} = \frac{N_{OH}}{N_{H_2}} \approx 5 \times 10^{-5}\left(\frac{300\ \text{K}}{T}\right)\left(\frac{10^5\ \text{cm}^{-3}}{n_{H_2}}\right)^{4/3}$	
Volume filling factor	$\Phi_v \approx 0.03$–0.1	

gas is $\Phi_A = \Phi_v^{2/3} = 0.16^{+0.15}_{-0.08}$. The corresponding cloud radius is $R_c \sim \Phi_v^{1/3} R \sim 0.8$ pc $= 16''$. If the cloud sizes were similar to those of the ionized gas ($R_c \sim 2''$–$6''$; Lacy *et al.* 1980; Lo and Claussen 1983), the beam filling factor would be between 0.1 and 1.

Thus, the neutral gas in the galactic center is highly clumped filling only about 10% of the volume. This clumping is consistent with the cloud structure of the ionized gas (Lacy *et al.* 1980; Lo and Clausen 1983; Serabyn and Lacy 1985), and consistent with the "spiky" appearance of the 21 cm H I velocity profiles taken toward individual positions at high spatial and spectral resolution (Liszt *et al.* 1983). The parameters of the neutral atomic gas near Sgr A are summarized in Table 2.

e) OH *Absorption Lines*

Figure 4*b* shows the detection of 119 μm OH absorption from the ground state toward Sgr A West and, for comparison, toward Sgr B2. The OH absorption in the Galactic center is centered at -80 km s^{-1}, and its width is significantly greater than the spectral resolution. This absorption probably does not originate in the central 5 pc, since Sgr B2 ($\Delta l \sim 0.^\circ5$) shows a similar blueshifted absorption line whose centroid (-40 km s^{-1}) is different by 90 km s^{-1} from the intrinsic velocity of the Sgr B2 complex. The similarity of the velocity centroids in the two sources suggests that the OH absorption comes from cool, optically thick gas in the "expanding molecular ring" which is in front of the Galactic center and at galactocentric radii of several 10^2 pc (e.g., Liszt and Burton 1980; Güsten and Downes 1980). The "molecular" ring has velocities approximately matching those of the OH lines toward Sgr B2 and Sgr A. The 119 μm optical depth derived from the data in Figure 4*b* and corrected for the finite spectral resolution is large ($\tau_{119} > 2$ and most likely $\gg 2$), consistent with the 1.7 GHz radio observations of OH (e.g., Bieging 1976; $N_{OH} \sim 10^{17}$ cm^{-2}) and low-temperature gas (see Storey, Watson, and Townes 1981).

f) *Far-Infrared Molecular Gas Emission*

Besides emission from atomic gas, there are also emission lines from excited CO and OH molecules toward the central 1′ of the neutral gas ring. In addition to the spectrum at $\Delta l = -40''$ containing the $J = 16 \rightarrow 15$ CO line and the two $^2\Pi_{1/2}$, $J = 3/2 \rightarrow 1/2$ OH lines (Fig. 4*a*), the CO line was observed at two additional positions ($\Delta l = 0$, $\Delta l = +40''$, Fig. 7). The CO velocity centroids are blueshifted by 50–100 km s^{-1} at $\Delta l = -40''$, and are redshifted by about the same amount at $\Delta l = +40''$, similar to the [O I] and [C II] lines (see Paper I and § III*h* below). Hence, the CO emission almost certainly arises in the central 5 pc of the Galaxy. It is not as certain that the OH emission also originates in the same region. At the $\Delta l = -40''$ position, the OH emission lines have about the same line-center velocity as the CO and fine-structure lines, suggesting that these lines also come from the rotating ring.

g) *Excitation of the Molecular Gas*

Since only one CO and one OH transition were observed, the data are not sufficient to determine fully the state of the molecular gas. In the following, we derive constraints on the column density and abundance of CO and OH. The derived parameters of the molecular gas are summarized in Table 2.

i) CO *Emission*

The excitation of the $J = 16$ level of CO is through collisions, and it is clear that fairly high densities and temperatures

are required to produce the observed far-infrared emission. Optically thin emissivities as function of density and temperature have been computed by McKee *et al.* (1982). The observed value of $I_{CO} = 1.5 \times 10^{-4}$ ergs s^{-1} cm^{-2} sr^{-1} then implies a beam-averaged column density of

$$N_{CO} \sim 1.3 \times 10^{18} \left(\frac{10^5 \text{ cm}^{-3}}{n_{H_2}}\right)^{1.25} \left(\frac{300 \text{ K}}{T}\right)^{3.1} \text{cm}^{-2}, \quad (3)$$

where we have approximated the CO emissivity as a power-law expression (correct to a factor of 2 between $10^4 \leq n_{H_2} \leq 10^6$ and $200 \leq T \leq 800$ K).

The CO emission may come from molecular gas within the photodissociation region with parameters similar to the [O I]/[C II] gas, or may come from a separate component of hot molecular gas excited by shock waves, similar to the far-infrared CO emission in Orion–KL (Storey *et al.* 1981). If the state of the molecular gas is similar to that of the atomic gas, there has to be a substantial column density of molecular material in the photodissociation region:

$$N_{CO}(n_{H_2} \sim 10^5, T \sim 300) \geq 10^{18 \pm 0.5} \text{ cm}^{-2} \approx N_{C^+}. \quad (4)$$

This column density corresponds to a CO/H_2 ratio of 6×10^{-5}, similar to those found in other molecular clouds. Because of the strong temperature dependence, the required CO column density decreases with increasing temperature, with $n_{H_2} T$ kept constant. The CO line is optically thin ($\tau_{163}^{CO} \sim$ a few $\times 10^{-2}$). As with the atomic gas, the volume filling factor of the $J = 16 \rightarrow 15$ emission must be low because of the high hydrogen volume densities and low hydrogen column density.

Perhaps more likely, the CO emission may come from hot, shock-excited gas with parameters similar to the Orion–KL shock ($n_{H_2} \sim 10^6$ cm^{-3}, $T \sim 750$ K [Storey *et al.* 1981; Watson *et al.* 1985*b*]). At $T = 750$ K, the required CO column density ranges between 7.5×10^{15} and 7.5×10^{16} cm^{-3}, and a relatively small abundance of warm CO relative to molecular hydrogen is required ($[CO]/[H_2] = 4 \times 10^{-7}$ and 4×10^{-6}). We note that in either of these cases the inferred CO abundance is not high enough to solve the lack of gaseous carbon and oxygen discussed above. To fully account for that deficiency, the $J = 16 \rightarrow 15$ emitting CO gas has to have temperatures significantly lower than 300 K, or an additional large amount of cool CO has to be present.

ii) OH *Emission*

Detection of the 163 μm rotational emission lines of OH is unexpected, since it implies a large column of OH in the neutral gas disk. We find that the abundance of OH toward the southern [O I] peak is probably between 10^{-7} and 10^{-5}, larger than is generally found in cooler molecular clouds ($\chi_{OH} \sim 10^{-9}$–10^{-7}) or expected from standard ion-molecule chemistry (e.g., Prasad and Huntress 1980). This conclusion applies whether the excitation mechanism is collisional or radiative, as is discussed in the Appendix. In the case of collisional excitation, the densities required are at least as high as in the case of the atomic gas and CO.

h) Kinematics of the Neutral Gas

The data presented here confirm the conclusion of Paper I: that the kinematics of the neutral gas within $R \leq 5$ pc is dominated by rotation around the center. The new observations define this axis to be within 20° of the Galactic rotation axis. The higher quality of these data permit an improved determination of the kinematics and the mass distribution.

The [O I] and [C II] profiles shown in Figures 1–3 are clearly resolved at most positions. The lines are widest close to the center, $\Delta v_{FWHM} \sim 200$–400 km s^{-1}, well in excess of the instrumental resolution (100 km s^{-1}). Farther out, the lines become narrower ($\Delta v_{FWHM} \sim 140$–160 km s^{-1}). There is no evidence for the wide [O I] lines at $\Delta l = \pm 80''$ reported in Paper I. The profiles of the different fine-structure lines at common positions are very similar, further strengthening our conclusion that the lines come from the same gas component. The OH lines shown in Figure 4 also do not differ significantly from the fine-structure lines at the same positions. However, the CO line toward the southern peak in Figure 4 appears to be narrower ($\Delta v_{FWHM} = 185 \pm 30$ km s^{-1}) than either the average of the OH lines (235 ± 40 km s^{-1}) or the [O I]/[C II] lines (250 ± 20 km s^{-1}). The CO line at $\Delta l = 0$ may also be somewhat narrower than the fine-structure lines, but the CO width at $\Delta l = +40''$ is consistent with the atomic emission. The smaller spread in velocities may indicate that the CO emission comes from a smaller region than the OH and fine-structure emission, or from a region farther away from the center.

Figure 9 is a longitude-velocity diagram of the [O I] data at 30″ spatial and 100 km s^{-1} spectral resolution along the Galactic plane ($\Delta b = 0$). Figure 10 shows maps of the [O I] emission at different velocities in the innermost region constructed from the 30″ data only. The maps and the *l-v* diagram indicate that the [O I] emission comes from a *rotating disk or thick ring* of inner radius $R_i \sim 2$ pc and outer radius a few times the inner radius. In an *l-v* diagram a very thin, rotating ring (rotation axis perpendicular to the Galactic plane) at inclination angle i and tilted by φ relative to the Galactic plane transforms into a straight line, whose endpoints give the rotational velocity times sin i and the radius of the ring times cos φ. The slope of the line is the ratio of rotational velocity to the radius times sin i/cos φ. The [O I] data in Figure 9 give

$$R_i \cos \varphi = 1.5\text{–}2 \text{ pc} = 30''\text{–}40'',$$

$$\frac{v_{rot} \sin i}{R_i \cos \varphi} = 48 \pm 10 \text{ km s}^{-1} \text{ pc}^{-1} = 2.4 \pm 0.5 \text{ km s}^{-1} \text{ arcsec}^{-1}. \quad (5)$$

Hence, the projected rotational velocity at 2 pc is $v_{rot} \sin i = 95 \pm 7$ km s^{-1}. As discussed in § III*a*, the tilt is $\varphi = -20°$. This rotational velocity has been derived mostly from the data at negative longitudes, since there are larger deviations from the simple picture of a rotating ring at positive longitudes. The rotational velocity determined from velocity centroids in a disk of *finite* thickness, as is the case for the Galactic center, is a *lower* limit to the true rotational velocity due to lower projected velocities from gas at different radii (see discussion in Paper I). However, the [O I] emission at the inner edge is much stronger than at larger radii. Hence, the [O I] emission is similar to that of an unresolved thin ring. The velocity centroids decrease by 10%–40% between the inner edge and $R \sim 100''$ (5 pc), where the [O I] intensity has decreased to about 10% of its peak value (see the velocity centroids in Fig. 9).

i) *Noncircular Motions*

There are obvious deviations from the motions of a rotating disk. The spectra close to the center are very broad ($\Delta b = 0$, $\pm 20''$ in Fig. 1), and the central spectrum is double-peaked. Since the inner diameter of the disk is well resolved by the 30″ beam, the expected emission at $\Delta l = 0$ should come from low-

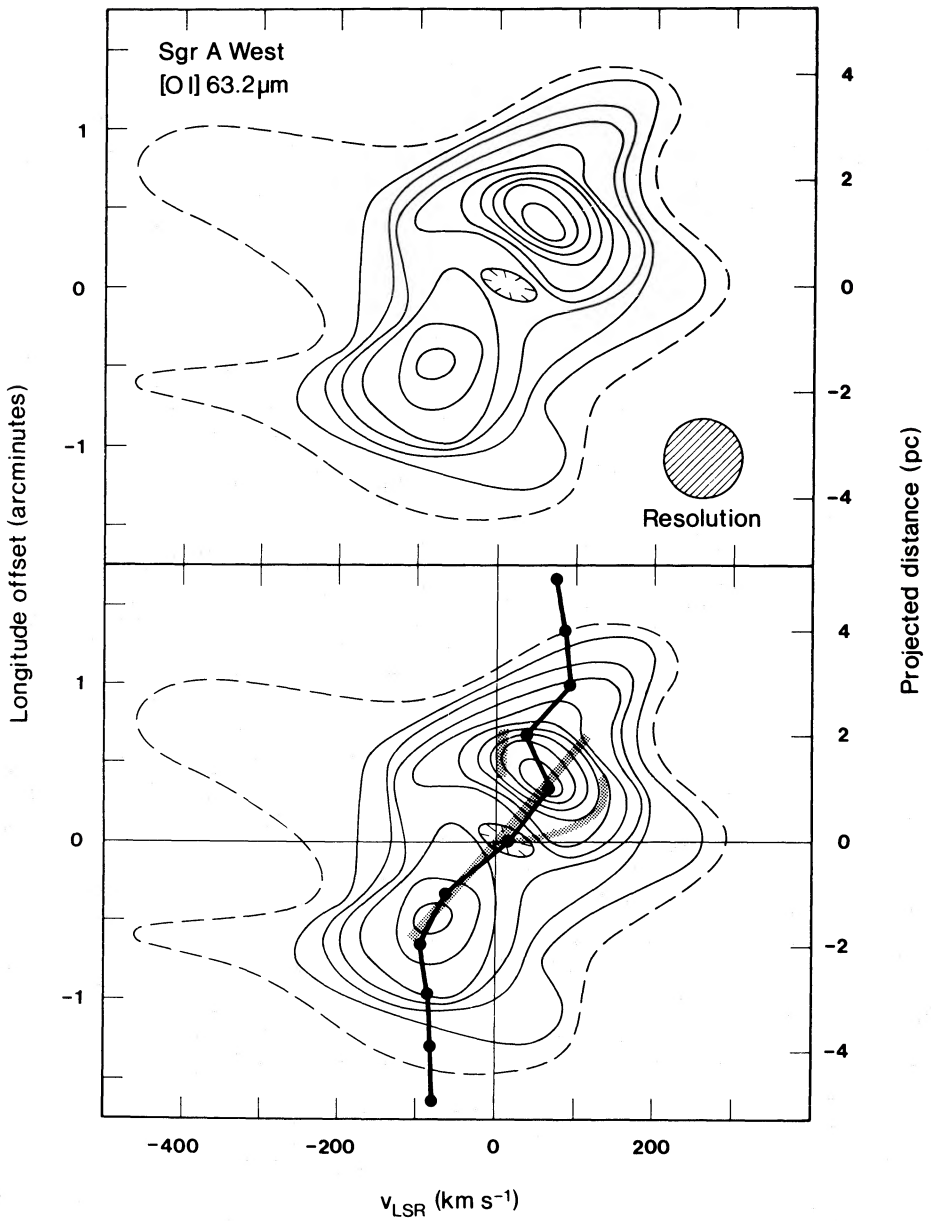

FIG. 9.—(*Top*) The *l-v* diagram of the [O I] 63 μm emission along the Galactic plane; relative to the base position in Fig. 5 (100 km s^{-1} and 30″ resolution). Contours are multiples of 2.4 × 10^{-18} W cm^{-2} per resolution element or 9 × 10^{-4} ergs s^{-1} cm^{-2} sr^{-1} per resolution element. (*Bottom*) Superposed on the [O I] *l-v* diagram are the [O I] line centroids (*filled circles and heavy lines*), which have a typical 1 σ uncertainty of ±5 to ±15 km s^{-1}. The stippled bars schematically represent the [Ne II] *l-v* diagrams of the western arc (linear feature stretching from $\Delta l = -35''$ to $\Delta l = +35''$), the northern arm (parabolic feature stretching from $\Delta l = 0''$ to $\Delta l = +30''$), and a zero-velocity feature at $\Delta l = +40''$ (data from Serabyn and Lacy 1985).

velocity material in front and behind the Galactic center, and the line should be narrow. Figure 10 shows that the emission at +100 and −100 km s^{-1} is concentrated toward the lobes on either side of the center, and that the emission near zero velocity is extended over the whole mapped area, as expected for a nearly edge-on rotating disk. In contrast to a rotating disk, however, the emission at +200 km s^{-1} peaks close to the center of the source, toward the "northern arm" of the free-free radio continuum emission (see Fig. 5 for an explanation of this feature). Blueshifted [O I] emission (−200 km s^{-1}) has a peak at $(\Delta l, \Delta b) = (+20'', +20'')$, west of the northern arm. The same features (high positive velocities near the center and negative velocities at $\Delta l = 10''$–$30''$) can also be seen in the *l-v* diagram of Figure 9. Furthermore, the peak velocity of the [O I] profile at $\Delta l = +40''$ is +30 km s^{-1}, which is inconsistent with the expected velocity of a rotating disk at that position. Finally, at larger distances from the center ($\Delta l = +40''$ to $+80''$), the line profiles are still fairly wide, and there is gas redshifted by 20–50 km s^{-1} at all negative longitudes in the [O I] and [C II] profiles (Figs. 1, 2, 3, and 9). These noncircular motions may have several causes. Some of the irregular motions near the center may be due to [O I] gas emission which is not located in the rotating disk but is associated with the ionized gas in the inner cavity. The evidence for this conclusion is discussed in the next paragraph. The fairly wide line widths may be caused by cloud-cloud turbulence in the neutral

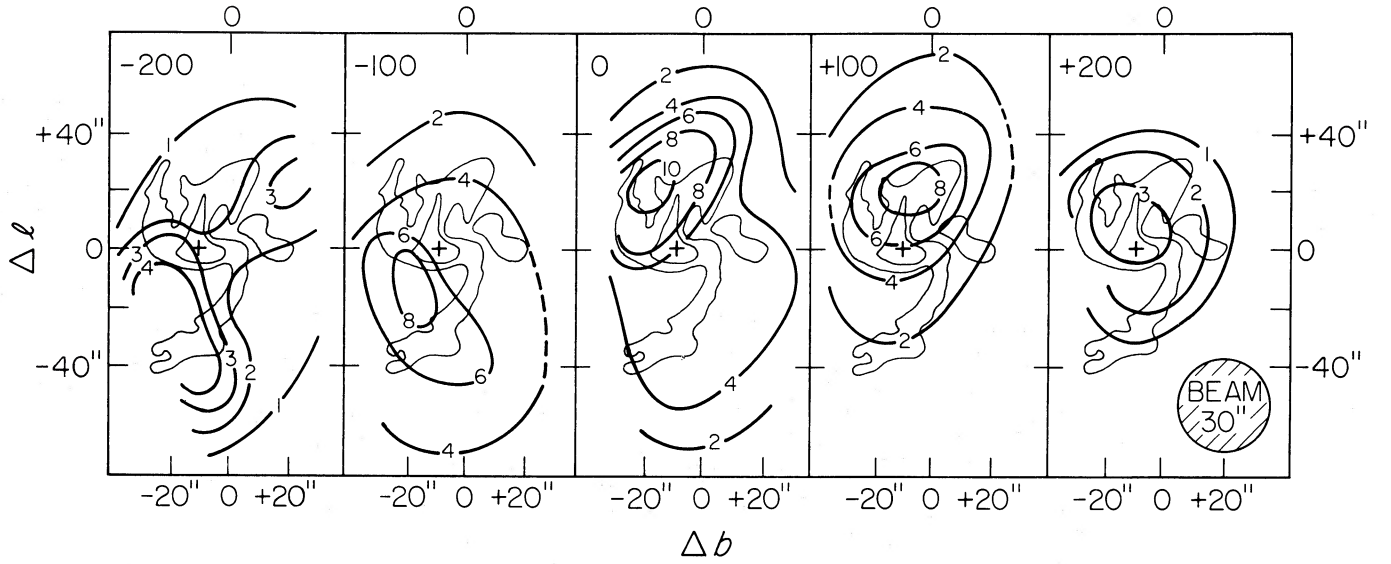

FIG. 10.—Shown are 30″ maps of [O I] emission in the innermost region at different LSR velocities (indicated at the upper half of each map), superposed on 2 cm radio continuum emission (Ekers *et al.* 1983). The cross marks the location of the radio point source. Contours are in units of 2.6×10^{-18} W cm^{-2} or 9.6×10^{-4} ergs s^{-1} cm^{-2} sr^{-1} per resolution element.

disk. Redshifted gas between +20 and +50 km s^{-1} could also come from Galactic molecular clouds centered a few arc minutes east of the Galactic center. Some of the noncircular motions may also be the response of the gas to a nonaxisymmetric potential, as is discussed in § IV*e*.

ii) *Comparison with Kinematics of Ionized Gas*

Many of the kinematic features present in the [O I] data are also characteristic of the 12.8 μm [Ne II] data of Lacy *et al.* (1980) and Serabyn and Lacy (1985) and the H76α recombination line data by van Gorkom, Schwarz, and Bregman (1984). This strongly suggests that the neutral, photodissociated gas and the ionized-gas components are closely related.

In the lower diagram of Figure 9, we compare the [O I] *l-v* diagram with that of the velocity centroids of the [Ne II] emission along the "western arc" and the "northern arm" (Serabyn and Lacy 1985; see Fig. 5 for an explanation of these features on the radio continuum map). The linear velocity gradient and maximum terminal velocity along the western arc are in excellent agreement with the parameters of the [O I] emission at the inner edge of the neutral rotating disk. Thus the western arc and the inner edge of the neutral disk are at about the same radius. The northern arm of the ionized gas and the localized cloud at $v_{LSR} \sim 0$ and $\Delta l \sim +30''$ may be correlated with some of the [O I] components deviating from the simple, rotating disk. Finally, the blueshifted [O I] emission at $\Delta l = +20''$ and $\Delta b = 0''$ and $+20''$ may correspond to a region of blueshifted [Ne II] emission in the "bar" west of the "spiral" (Serabyn 1984). The close correspondence between the ionized and neutral gas kinematics is further strengthened by the good agreement of the [O I] profiles with the [Ne II] profiles when the latter are averaged over 30″ regions at different positions in the central 2 pc (Serabyn 1984).

IV. DISCUSSION

a) Gas Heating Mechanisms

Figure 11 is a schematic spectrum of the line and continuum radiation from the central 2–3 pc of the Galaxy. This spectrum illustrates the high brightness of the far-infrared emission lines from the neutral atomic gas (O^0, C^+), relative to the infrared emission lines from ionized gas and the radio emission lines. The total luminosity of the atomic lines toward the central 2–3 pc is about $4 \times 10^3\ L_\odot$, and the line luminosity is $(3–6) \times 10^4\ L_\odot$ integrated over the source. In the Galactic center, as in the nuclei of bright infrared galaxies with a high rate of star formation, the far-infrared emission lines of C^+ and O^0 account for about 0.5% of the total bolometric luminosity and are very important cooling lines for the interstellar gas (Crawford *et al.* 1985). In addition to the atomic and ionic lines, submillimeter *molecular* line emission, especially from CO rotational transitions, significantly contribute to the gas cooling in the Galactic center. Extrapolating from the intensity of the $J = 16 \rightarrow 15$ line, the total CO rotational cooling in the submillimeter wavelength region may range from $\sim 1/10$ of the atomic cooling (if the CO emission comes from gas at $T \sim 750$ K) to an amount equivalent to or even exceeding the O^0/C^+ cooling (if the CO emission comes from gas at $T \leq 300$ K).

The neutral atomic gas in the ring is heated by nonionizing UV radiation ($912 < \lambda < 3000$ Å) from the Galactic center, rather than by shocks (see Paper I). However, the molecular gas that gives rise to the infrared H_2 lines and the CO $J = 16 \rightarrow 15$ line seems more likely to be shock-heated. These two conclusions are illustrated in Table 3, where the line emission from Sgr A is compared with that in the Trapezium and KL regions in Orion and to that predicted by a model for UV-heated photodissociation regions (Tielens and Hollenbach 1984*a*, *b*). There is good agreement in the [O I] and [C II] line ratios, atomic gas and dust temperatures, and the ratio of far-infrared line luminosity to total luminosity for Sgr A and Orion. A comparison between Sgr A and Orion is particularly useful, since the Orion-Trapezium interface region is a well-studied prototype photodissociation region (heated by stars of known total luminosity and type), and since the UV energy densities in the two objects are similar. The standard dissociation region model by Tielens and Hollenbach is fairly successful in accounting for the properties of the dust and atomic gas in both regions. However, the infrared H_2 and far-infrared

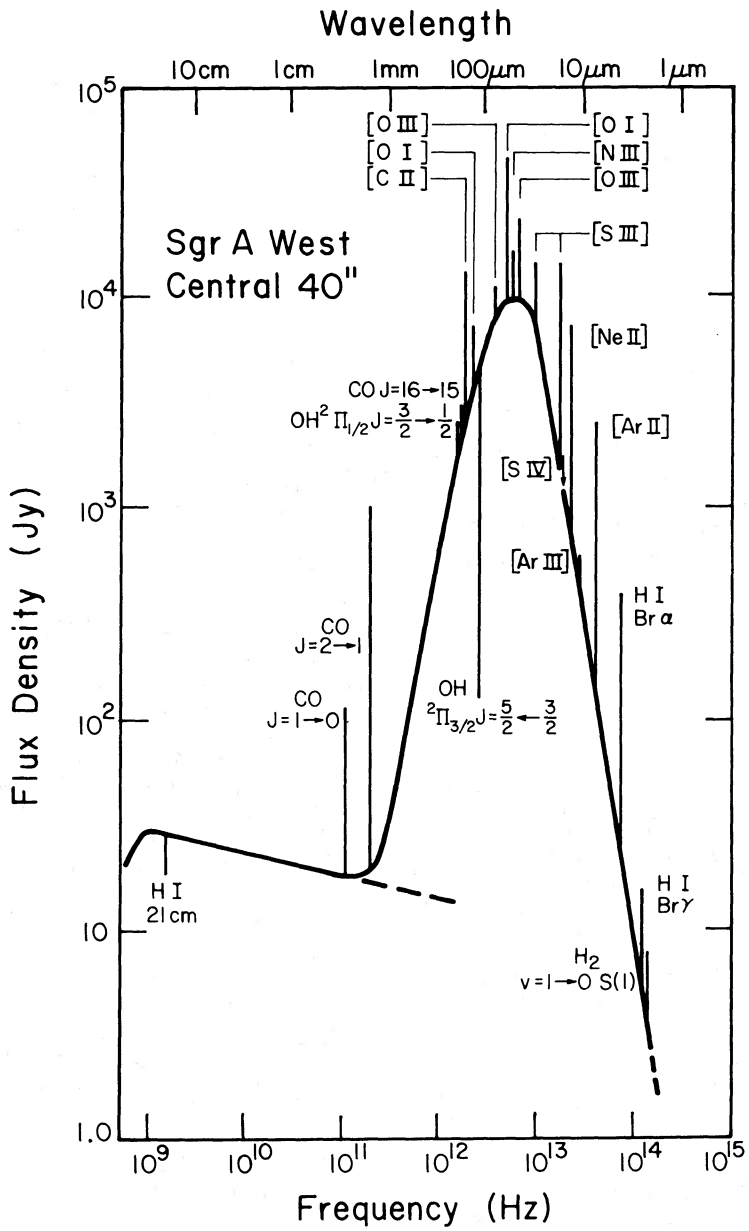

FIG. 11.—Schematic infrared and radio spectrum of line and continuum emission in the central 40″ (2 pc) of Sgr A West. Continuum data are from Rieke, Telesco, and Harper (1978), BGW, Ekers *et al.* (1983); the CO $J = 1 \rightarrow 0$ and H I data are from Liszt, Burton, and van de Hulst (1984); the CO $J = 2 \rightarrow 1$ data are from K. Y. Lo (1984, private communication); the 50–200 μm lines are from this paper and from Watson *et al.* (1985*a*); the mid-IR fine-structure line data are from Lacy *et al.* (1980) and the [S III] lines are from Herter *et al.* (1984); and the H_2 $S(1)$ data are from Gatley (1983) and Gatley *et al.* (1984).

CO emission in both Sgr A and Orion are 10–1000 times brighter than expected from the Tielens and Hollenbach model, and the gas temperatures derived from the H_2 lines in the two objects are similar to each other and substantially different from that in photodissociated matter. In Orion–KL it is well known that the H_2 and far-infrared CO emission arises in shocked molecular material near the core of the Orion molecular cloud (cf. Beckwith *et al.* 1978; Watson *et al.* 1985*b*) rather than from the photodissociation region. Shocked molecular material could also produce these lines in Sgr A, which could be dissipated in this fashion through cloud-cloud collisions within the neutral ring or through the interaction of this ring with a mass outflow from the Galactic center. This will be discussed further below (§§ IV*d*, *e*).

b) The Neutral-Gas Disk around Sgr A West

The far-infrared data presented in this paper, in BGW, in Paper I, and the radio observations by Liszt *et al.* (1983) and Liszt, Burton, and van de Hulst (1984) clearly demonstrate that there is an extensive rotating, neutral-gas and dust disk around the Galactic center. These measurements and the observations of the ionized gas (cf. Lacy *et al.* 1980; Lacy, Townes, and Hollenbach 1982; Ekers *et al.* 1983; Lo and Claussen 1983; van Gorkom, Schwarz, and Bregman 1984; Serabyn and Lacy

TABLE 3

GAS HEATING AND COOLING IN SAGITTARIUS A: COMPARISON WITH ORION AND PHOTODISSOCIATION REGION MODEL

Parameter	Sgr A	Orion	Model Photodissociation Region (TH 1984)	Remarks
L_{UV} ($L_\odot$)	$\sim 10^7$	$\sim 10^5$	...	1
ϵ_{UV} (6×10^{-13} ergs cm^{-3})	5×10^4	1.5×10^5	10^5	
L_{Line}/L_{UV}	5×10^{-3}	5×10^{-3}	10^{-2}	
$I_{[O\ I]63}/I_{[O\ II]158}$	19 ± 6	12 ± 4	29 (12)	2, 3
$I_{[O\ I]63}/I_{[O\ II]145}$	30 ± 9	26 ± 8	23 (13)	
T_{gas} (O I, C II)	350^{+650}_{-150}	350^{+650}_{-150}	300 (100–1000)	
T_{dust} (far-IR)	50–60	~ 80	~ 80	
$I_{CO\ 16\to 65}/I_{[O\ I]63}$	$(6 \pm 3) \times 10^{-3}$	$(100 \pm 50) \times 10^{-3}$	$\sim 0.5 \times 10^{-3}$	4
$I_{H_2\ S(1)}/I_{[O\ I]63}$	$(60 \pm 30) \times 10^{-3}$	1 ± 0.5 (KL) 10^{-2} (trap)	3.5×10^{-3}	
$I_{CO\ 16\to 15}/I_{H_2\ S(1)}$	0.1–0.2	0.3 ± 0.1 (KL)	0.2	5
T_{H_2} (2 μm)	2000	2000	~ 300–1000	
T_{CO} (far-IR)	...	750–1000	100–300	

REMARKS.—(1) Model values given are from the Tielens and Hollenbach 1984*a*, *b* (TH 1984) standard model ($n_H \approx 10^5$ cm^{-3}); values in parentheses represent a "best-fit" model where dust-to-gas ratio is adjusted to best fit the observations of Orion. (2) Orion data are from Ellis and Werner 1985 for [O I], [C II]; Stacey *et al.* 1982 for CO $J = 16 \to 15$; Watson *et al.* 1985*b* for CO $J = 16 \to 15$ and OH; Beckwith *et al.* 1978 for H_2; Gautier 1979 for H_2. (3) Sgr A data are from this paper for [O I], [C II], CO, OH; Gatley 1983 and Gatley *et al.* 1984 for H_2; BGW and Gatley *et al.* 1978 for far-IR continuum. (4) For Orion: upper value for H_2 to [O I] in Orion–KL shock (2 mag extinction); lower value for Orion-Trapezium and bar photodissociation region (no extinction correction). (5) H_2 data are dereddened for 3 mag at 2 μm in Sgr A and 2 mag at 2 μm in Orion–KL.

1985) give a consistent and fairly detailed picture of the structure of interstellar gas in the central 10 pc which we will now summarize. Going outward from the center, one finds the following.

i) *Ionized Cavity* ($R \leq 1.5$ pc)

This region includes the He I zone around IRS 16 and the radio point source (a few arcsec diameter: Geballe *et al.* 1984; Hall, Kleinmann, and Scoville 1982), the bar structure with the highest velocity (± 260, ± 140 km s^{-1}) [Ne II] motions and probably the northern arm (Serabyn and Lacy 1985; Serabyn 1984). The ratio of the two [O III] lines at 52 and 88 μm, the ratio of H I (Huα) to [Ne II] intensity, and the ratio of the two [S III] lines indicate that much of the ionized gas is very dense ($n_e \geq 2 \times 10^3$ cm^{-3} and likely 10^4–10^6 cm^{-3}; Watson *et al.* 1980; Paper I; Serabyn 1984; Herter *et al.* 1984). Any distributed ionized gas must have a density less than ~ 40 cm^{-3} (Watson *et al.* 1980). As a result, the volume filling factor of the ionized gas at $R \leq 1.5$ pc is very small ($\Phi_v \lesssim 10^{-2}$), and most of the UV escapes this zone (BGW; Lacy *et al.* 1980).

There is a significant amount of neutral gas in this inner region. The [O I] data give evidence for neutral atomic gas associated with the northern arm, and some indication for high–velocity-dispersion [O I] gas associated with the bar material. From the flux of high-velocity [O I] emission into a 30″ beam at the central position, we estimate an oxygen column density of $\sim 5 \times 10^{17}$ cm^{-2} and a total neutral-gas mass of $\sim 20\ M_\odot$ ($O^0/H = 6.7 \times 10^{-4}$). The total amount of ionized gas in the inner region ranges between 7 and 70 $M_\odot$, for electron densities of 10^5 and 10^4 cm^{-3}, respectively. A possible explanation is that some or most of the cloudlets visible on the radio continuum maps contain dense neutral cores but are ionized on their surfaces.

ii) *Inner Edge of the Neutral Disk* ($R \sim 1.5$–2 pc)

There is now convincing evidence that the ionized gas in the western arc of the radio continuum spiral is close to the edge of the neutral disk, and probably comes from clouds at the edge of the disk which are exposed to Lyc radiation. The main body of the [O I] emission and the ionized emission in the western arc appear to come from different sides of the inner edge of the disk (Fig. 5), and neither set of observations shows a full disk or ring structure. A possible explanation could be that the eastern part of the disk is more massive (hence more intense in [O I]) but that there are variations in the flux of ionizing radiation along the perimeter of the disk due to obscuration by dense gas between the disk and the center producing less [Ne II] there (Serabyn and Lacy 1985). An alternative is that the western arc is part of a tidally distorted, infalling streamer and, hence, does not form a complete ring (Quinn and Sussman 1985).

If the western arc and the [O I] arc in Figure 5 trace the two sides of the rotating disk, we estimate that the ring is inclined by $i = 69° \pm 5°$ relative to the line of sight (see also Liszt, Burton, and van de Hulst 1984). In this case it appears that the lateral extent of the [O I] emission of the disk is not significantly wider than would just be expected from the inclination; hence the Galactic center disk may be quite thin (thickness $\lesssim 1$ pc). The true rotational velocity estimated from the [O I] velocity centroids at $R_i = 40''$ is 102 ± 10 km s^{-1}. The 2 μm H_2 emission observed by Gatley (1983) and Gatley *et al.* (1984) also arises near the inner edge of the disk, but clearly peaking inside the disk.

iii) *Neutral-Disk* ($2 \leq R \leq 5$ pc)

Most of the [O I], [C II], and far-infrared dust emission originates at distances greater than 2 pc from the galactic center. This is the photodissociation zone where most of the (5–10) $\times 10^6\ L_\odot$ of UV radiation emanating from the Galactic center is absorbed. The [C II] emission extends deeper into the cloud than either the [O I] or the far-infrared continuum emission.

The $J = 1 \to 0$ CO emission peaks in a layer very close to the C^+ region. Both regions appear to overlap considerably.

The H I 21 cm optical depth is largest very close to the CO peak and shows a very steep falloff toward the center. At the [O I] and dust continuum peaks the H I optical depth has dropped to about $\sim 25\%$ of its maximum value.

There is a considerably amount of warm or hot molecular gas (CO, OH, H_2) mixed with the atomic gas. This high abundance may suggest that molecular and atomic gas are coexistent throughout the region.

While the first two findings are in good agreement with the theoretical predictions for a photodissociation region, the latter two appear to contradict theory. In the models, the neutral, atomic hydrogen arises in a narrow layer (A_v: 0 to ~ 2) at the outermost surface of the cloud. Both C^+ and O^0 persist deeper into the cloud than H I. Even if the observation by Liszt *et al.* (1983) were corrected for a steep temperature gradient toward the center (T_{spin} rising to ~ 300 K at $R = 2$ pc), which would bring the H I column density at the [O I]/dust peaks to $N_{HI} = 2 \times 10^{22}$ cm^{-2}, there would still be an approximately constant hydrogen column density extending far into the cloud ($A_v \sim 10$), farther than the C^+/O^0 zone. In addition, the models by Tielens and Hollenbach (1984*a*, *b*) predict that most gaseous carbon is in C^+, and very little in CO.

The explanation of this apparent contradiction between data and theory and of the large thickness of the photodissociation region is probably the clumpy structure of the cloud. While any one clump is optically thick in the UV, the UV radiation can penetrate on average quite deep into the cloud, which has a volume filling factor $\lesssim 10\%$. In such a clump the linear size of the photodissociation region on the side facing the UV source ($\Delta A_V \sim 5 - 10^{22}$ cm^{-2}) is only about 0.03 pc, or 0".6. If the clump sizes observed for the ionized gas (2"–10") are also typical of the neutral gas, the photodissociation region is only a thin skin on the surface of each clump. As a consequence, molecular material may be expected to exist very close to the inner edge of the neutral ring, while the UV radiation can penetrate far into the cloud.

The spatial distributions of all radio and infrared lines qualitatively suggest that some combination of heating, gas temperature, density, and column density decreases radially outward on the scale of a few pc. Beyond $R \sim 4$ pc, the gas is probably predominantly molecular.

iv) *Gas beyond* 5 pc?

There is currently no information on the continuation of the disk beyond the outer contours of the CO $J = 1 \rightarrow 0$ clouds at ± 100 km s^{-1} observed by Liszt *et al.* (1983), mainly because of confusion with other molecular material located along the line of sight to the center, but not at the center. The molecular clouds at $+20$ and $+50$ km s^{-1} are located at projected distances of 10–20 pc from the center, but have commonly been interpreted as being much farther away (e.g., Güsten and Downes 1980; Brown and Liszt 1984).

c) Mass Distribution in the Central 5 pc

The gas motions at $R \geq 2$ pc are dominated by rotation. The [O I] velocities, therefore, give an estimate of the mass distribution in the Galactic center. The rotational velocity at $R = 2$ pc, the inner edge of the neutral disk (102 ± 10 km s^{-1}, corrected for 69° inclination), corresponds to an enclosed mass of $(4.8 \pm 1.0) \times 10^6\ M_\odot$. The [O I] velocity centroid at $R = 3$ pc is 80 ± 10 km s^{-1} [$(4.4 \pm 1.1) \times 10^6\ M_\odot$] and at 4.5 pc is 79 ± 15 km s^{-1} [$(6.5 \pm 2.5) \times 10^6\ M_\odot$]. These values are plotted in Figure 12 as a function of distance from IRS 16.

The rotational velocity and inferred mass enclosed within 2 pc are in excellent agreement with the [Ne II] data in the western arc at $R = 1.7$ pc ($4.7 \times 10^6\ M_\odot$; Serabyn and Lacy 1985). The [O I] velocities at 3–4.5 pc also agree well with the CO $J = 1 \rightarrow 0$ velocity centroid of the blueshifted CO peak at $R = 4$ pc (-83 ± 7 km s^{-1}; Liszt, Burton, and van de Hulst 1984). We note, however, that both the [O I] and the CO emission at projected radius of $R \geq 2$ pc probably come from gas at various radii. In this case, the velocity centroid is not always a good measure of rotational velocity. Instead, the terminal velocity, that is, the high-velocity edge of the profile, may be a better measure of the rotational velocity. This correction probably does not affect the bright [O I] emission at the inner edge ($R = 2$ pc), but may increase the rotational velocities at $R > 2$ pc by 10%–40%. The correction for the [O I] velocities is rather uncertain because of the relatively low velocity resolution and the influence of noncircular motions. To indicate the possible magnitude of the effect, the open and filled triangles in Figure 12 given the rotational velocities at 4.5 pc, determined from the edges and centroids, respectively, of the CO data by Liszt *et al.* (1983).

The [O I] velocities by themselves are consistent either with an isothermal stellar cluster, where the rotational velocity is

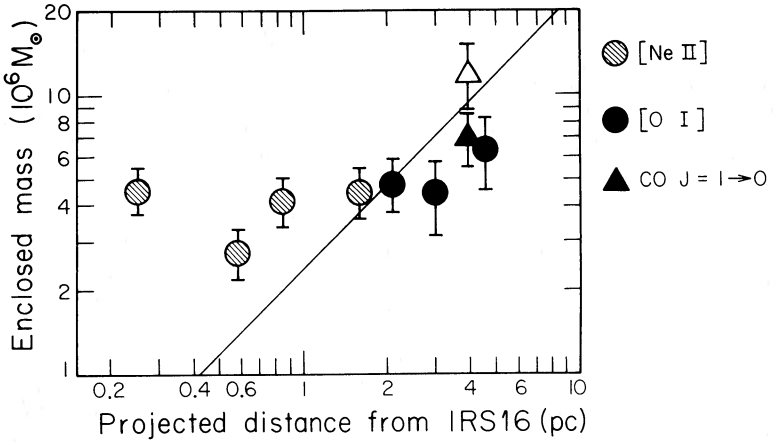

FIG. 12.—Enclosed mass as a function of distance from IRS 16. The masses were derived from the velocities of neutral and ionized gas, assuming circular orbits: $M = v^2R/G$. The [O I] data are from this paper, the CO $J = 1 \rightarrow 0$ data from Liszt *et al.* (1983, 1984), and the [Ne II] data from Lacy *et al.* (1980; inner two points, from the bar) and Serabyn and Lacy (1985; outer two points, from the northern arm and western arc). For the CO data, both the velocity centroid (*filled triangle*) and terminal velocity at the half-power point (*open triangle*) are given. All observed rotational velocities at ≥ 1.5 pc come from the rotation ring and are corrected for an inclination of 69°. The thin diagonal line represents the mass distribution of a stellar cluster with $\sim 5 \times 10^6\ M_\odot$ enclosed in 2 pc. The observed [Ne II] velocities of Lacy *et al.* (1980) do not require as support a massive central object if the clouds have fallen from an initial distance much larger than their current distance from the center or if their motion is radially outward.

constant and the enclosed mass increases linearly with radius, or with a point mass, where the rotational velocity decreases as $R^{-1/2}$. The strongest constraint on the mass distribution comes from a comparison between the [O I] and [Ne II] measurements.

Lacy *et al.* (1980) have measured the velocities of 14 [Ne II] clouds at projected distances between 0.2 and 1.5 pc from IRS 16. There are two clouds at ± 260 km s^{-1} LSR velocity at about 0.2 pc radius. Three clouds at an average distance of 0.6 pc have a velocity of ~ 140 km s^{-1}. These latter five clouds are in the bar (Fig. 5). The [Ne II] velocities in the northern arm reach a terminal velocity of 140 km s^{-1} at ~ 0.85 pc distance from IRS 16 (Serabyn and Lacy 1985). *If these velocities are interpreted as circular motion,* and are combined with the [O I]/[Ne II] rotational velocity at the inner edge of the neutral disk, then 40%–100% of the $\sim 5 \times 10^6\ M_\odot$ contained within 2 pc must also be contained in a region of $\lesssim 0.4$ pc (8″) in diameter (see Fig. 12). Such a mass concentration is inconsistent with a spherical, isothermal stellar cluster, and requires a central point mass or an unusual, nonspherical or non-thermalized stellar cluster. The high-velocity He I/H I gas detected within a few arcsec of IRS 16 would also be consistent with circular motions around such a point mass (Geballe *et al.* 1984).

The situation is more complex if the inner ionized clouds have a substantial noncircular component of motion. In general, the enclosed mass required for a given velocity is then *less* than the mass required for pure circular motion. For example, the mass required by the inner [Ne II] clouds in Figure 12 would decrease by a factor of 2 if these clouds were falling freely in with a point mass at the center. The factor is $2 \ln (R_o/R)$ if the clouds have been falling freely in from an outer radius R_o, with initial velocity zero, to their present radius R in the gravitational field of a stellar cluster whose density varies as r^{-2}. For example, if the ± 260 km s^{-1} clouds had fallen from the outer edge of the neutral ring to their present position, R_o is $\lesssim 8R$, and the required mass enclosed within $R \leq 0.25$ pc is $> 1 \times 10^6\ M_\odot$. This mass is still greater than but near to the mass expected if one extrapolates from the enclosed mass at 2 pc assuming that the stellar density varies as r^{-2}. No point mass is required in this case for some of the other [Ne II] clouds. Hence, *the observed* [Ne II] *velocities of Lacy et al (1980) do not require a massive central object if the clouds have fallen from an initial distance much larger than their current distance from the center.* The observed motions also do not require the presence of a massive central object if the clouds are expanding from the center. In this case, however, the source or sources of mass outflow have to provide the energy for a mass outflow rate of $\sim 10^{-3}$–$10^{-4}\ M_\odot$ yr^{-1}, which may require the presence of one or several massive objects at the center. There is also other evidence for a point mass at the center. A detailed analysis of the kinematics of the northern arm suggests that this feature is a coherent gas filament in a parabolic or hyperbolic orbit in the gravitational field of a point mass of (3–5) $\times 10^6\ M_\odot$ (Serabyn and Lacy 1985).

d) Stability of Clouds in the Neutral Disk

The clouds in the neutral-gas disk are subject to stripping by strong tidal forces and to frequent cloud-cloud collisions. The Roche critical density for tidal stability is $\sim 10^7$–10^8 cm^{-3} at $R \sim 2$ pc, more than 2 orders of magnitude higher than the measured density of the neutral clumps. The mean cloud-cloud separation is $d_{cc} = (\Phi_v)^{-1/3} R_c \approx 0.2$–$0.6$ pc. Judging from the noncircular [O I] velocities and the cloud-cloud velocity variations in [Ne II], the velocity dispersion between clouds may be $\Delta v \sim 20$–50 km s^{-1}. The mean time between cloud-cloud collisions then is $\tau_{coll} \sim 5 \times 10^3$ to 3×10^4 yr. This is considerably shorter than the rotation period of clouds at the inner edge of the natural ring (10^5 yr), or the thermal expansion time scales ($\sim 10^5$ yr). Hence, a single cloud has a high probability of collisions with another cloud during one rotation around the center.

A significant fraction η_s of the kinetic energy of a cloud may be converted into radiation via shocks in a cloud-cloud collision. Assuming a total gas mass of $M_g = 10^4\ M_\odot$, one might then expect a radiative dissipation rate due to shocks of

$$L_{\rm shock} \sim \eta_s \frac{(1/2) M_g \Delta v^2}{\tau_{\rm coll}} \sim 4 \times 10^3\ L_\odot \left(\frac{\eta_s}{0.1}\right)\left(\frac{M_g}{10^4\ M_\odot}\right) \times \left(\frac{\Delta v}{30\ {\rm km\ s^{-1}}}\right)^2 \left(\frac{2 \times 10^4\ {\rm yr}}{\tau_{\rm coll}}\right). \quad (6)$$

Hence the dissipation of noncircular motions in cloud-cloud collisions may account for the H_2 emission observed by Gatley (1983) and possibly also for far-infrared CO and OH line emission.

Assuming that angular momentum can be transferred between clouds, tidal stripping and cloud-cloud collisions probably will cause material to fall into the center. An upper limit to the current mass inflow rate may be estimated from the amount of material in the bar or northern arm to be about 10^{-4}–$10^{-3}\ M_\odot$ yr^{-1} (Lo and Clausen 1983; Ekers *et al.* 1983). Under these circumstances, a good fraction of the neutral-gas disk around the center will have accreted onto the central region in 10^7–10^8 yr. This accretion process may be a transitory phase followed by active ejection from the center (Lo and Claussen 1983; Ekers *et al.* 1983), also re-exciting the turbulent material in the disk, or the material in the ring has to be replenished with gas from further out. One possibility is that the $+50$ and $+20$ km s^{-1} Galactic center molecular clouds are actually close to Sgr A and may feed material into the center (Ho *et al.* 1985).

e) Genesis of the Neutral Disk

How did the neutral disk form? In the preceding discussions, we have noted several features which must be accounted for in answer to this question. The disk is apparently a moderately stable, rather than transient, structure. However, it is quite clumpy, despite the fact that the critical tidal-disruption density greatly exceeds the densities found in the clumps, indicating a need for an additional compressive agent. Its inner boundary is well defined, and it surrounds a central "cavity" which is relatively devoid of gas. Although its motion is dominated by rotation, the disk appears to have substantial internal, noncircular motions. Shocked molecular material is distributed throughout the disk. Finally, it may be the progenitor of the partially ionized clouds seen near the center.

Perhaps the simplest explanation which one might propose for the formation of the disk is that of an explosive (e.g., supernova or explosive instabilities in accretion around a black hole) or eruptive (e.g., burst of star formation) event in the center of the Galaxy, which has removed gas from the central 2 pc. A single Type II supernova would provide enough energy to remove to large distances about 1000 $M_\odot$ of interstellar gas initially mixed in with the central cluster. There may have been too little angular momentum in this gas to provide that seen in

the present neutral ring, but the expanding gas could conceivably acquire the deficit by sweeping up a small amount of rotating gas at larger radii and settling back into orbits in the $r = 2$–5 pc range. This would not by itself lead to a very well-defined ring or to the observed noncircular motions, and thus seems much less likely than the alternative mechanisms.

Gaseous rings or disks which surround cavities are often explained as radiatively driven or wind-driven bubbles. The luminosity of the Galactic center is insufficient by many orders of magnitude for radiation pressure to be effective. However, a better case can be made for stellar-type winds, some evidence for which is found in the presence of high-velocity (~ 700 km s^{-1}) ionized gas associated with IRS 16. When this is interpreted as outflowing gas, a mass loss rate of 10^{-4}–10^{-2} $M_\odot$ yr^{-1} is implied (Geballe *et al.* 1984). This result, together with the 2 μm H_2 emission in the disk, led Gatley *et al.* (1984; see also Gatley 1983) to suggest that the cavity and disk comprise a mass loss bubble, the abrupt boundary of which arises from the balance of wind pressure and gravitation. The [Ne II] clouds near the center could have been produced from material in the disk by Rayleigh-Taylor instabilities in the wind shock, and the molecular hydrogen emission would come from shocked neutral ring material. A mass loss rate of 3×10^{-3} $M_\odot$ yr^{-1} or greater would account for the H_2 lines, if only a small (10%) fraction of the originally isotropic wind actually pushes on the neutral disk (Gatley *et al.* 1984). There are, however, dynamical problems with this model. Even if an increased central mass is considered, owing to wind support of the disk, the [Ne II] clouds would be buoyant in winds as strong as those described; since at least some of them appear to be falling in or to be in stable orbits around the center, the mass-flow rate cannot be greater than about 10^{-3} $M_\odot$ yr^{-1}. In this case, the wind may be dynamically unimportant and may not be able to provide the energy for the molecular hydrogen emission. In any case, a shock speed of 700 km s^{-1} in the neutral disk would produce an extensive ionized layer on the inner rim (see Shull and McKee 1979), which is not observed.

Perhaps a very promising means for the generation of the neutral disk is a purely dynamical one, of which the ring's strong differential rotation is suggestive. The flat rotational curve shows that orbits are allowed for which the frequencies of radial oscillations are resonant with harmonics of the rotational frequencies. In particular, an inner Lindblad resonance (ILR) is allowed by the motions of the neutral disk. This would be significant if there were any bimodal asymmetry in the mass distribution, such as a small oval, triaxial, or barlike distortion in the shape of the central stellar cluster. Judging from the tendency of rotating stellar disks to evolve quickly into stable oval- or barlike shapes in numerical experiments (e.g., Hohl 1971), and from the frequent occurrence of barred structures in the center of spiral galaxies (e.g., Freeman 1970), it seems plausible that the central cluster in our Galaxy could have a small asymmetry. As has been shown by several authors (e.g., Combes and Gerin 1984; Schwarz 1981), the intersection of orbits in the bimodally distorted gravitational potential leads to the rapid establishment of a spiral configuration in the surrounding gas. In this configuration, the rotating bar exerts torques on the gas clouds which are positive at radii larger than that of the corotation resonance (CR) and negative for smaller radii. The gas is then driven outward and inward from the CR and eventually becomes trapped in the orbits near the inner and outer Lindblad resonances, resulting in gas rings at these radii. Noncircular motions would be evident in these rings, and cloud collisions frequent. Thus a ring associated with a Lindblad resonance would appear to explain the salient features of the neutral disk in the Galactic center.

To illustrate the correspondence to the neutral disk, we have computed resonant orbits under the following assumptions:

1. The epicyclic approximation is valid.
2. The neutral disk is interpreted as an ILR.
3. The central star cluster is isothermal with a core radius much smaller than the disk, containing 5×10^6 $M_\odot$ within a 2 pc radius, so that the angular velocity of circular orbits is $\Omega = 100$ km s$^{-1}/R$ and the frequency κ for oscillation is given by

$$\kappa^2 = 2\Omega\left[\Omega + \frac{d}{dR}(R\Omega)\right] = 2\Omega^2 . \quad (7)$$

4. The stellar cluster has a small bimodal asymmetry.

The orbit resulting from a radial velocity amplitude of 85 km s^{-1} and positioned with its long axis perpendicular to the line of sight is shown in Figure 13*a*.[3] The longitude-velocity relation was then computed from this orbit by assuming the disk to be uniform and to have transverse extent and internal velocity dispersion much smaller than the instrumental spatial and spectral resolution, and convolving the emission of this disk with the instrumental response. Despite the numerous and gross assumptions, the model *l-v* relation shown in Figure 13*b* bears a striking resemblance to the observations.

V. CONCLUSIONS

We have reported mapping of far-infrared C^+ and O^0 fine-structure lines as well as the first detection of far-infrared CO and OH rotational line emission and OH absorption toward the Galactic center. These measurements have been compared with far-infrared and radio continuum maps, with recent observations of the 12.8 μm [Ne II] line, and with measurements of CO 2.6 mm emission and H I 21 cm absorption.

The new observations clearly show that there is a 10 pc diameter neutral-gas disk or torus of several times 10^4 $M_\odot$ surrounding the inner ionized cavity. The gas disk has an inner radius of 1.7 pc, is inclined by $\sim 69°$ relative to the line of sight, is tilted by $\sim -20°$ relative to the Galactic plane, and may be quite thin.

The atomic gas in the neutral disk is dense (10^5 cm^{-3}), warm ($T_{gas} = 300$ K $\geq T_{dust} = 50$ K) and fills less than 10% of the volume. Pressure, ionization, and excitation of the disk material decrease from the inner edge outward. Atomic and molecular material are mixed throughout the disk, and the inner surface of the disk is ionized by Lyc photons from the center. While the CO abundance in the Galactic center disk may be approximately the same as in other molecular clouds, and OH probably is overabundant, the *total* gaseous carbon and oxygen abundances (in C^+, O^0, CO, and OH) appear to be significantly below the solar abundances of these elements.

The most likely structure of the gas disk is that of a large number of small clumps in diameter 2″–10″ (0.1–0.5 pc). These clumps are largely ionized in the central cavity and at the inner edge of the disk, but contain a core of neutral atomic gas. Deeper into the cloud, only softer ($\lambda > 912$ Å) photons can penetrate. The UV radiation creates thin layers of photo-

[3] Although this velocity leads to a radial amplitude large enough to invalidate the epicyclic approximation, we do not expect the general appearance of the structure we compute to be seriously affected.

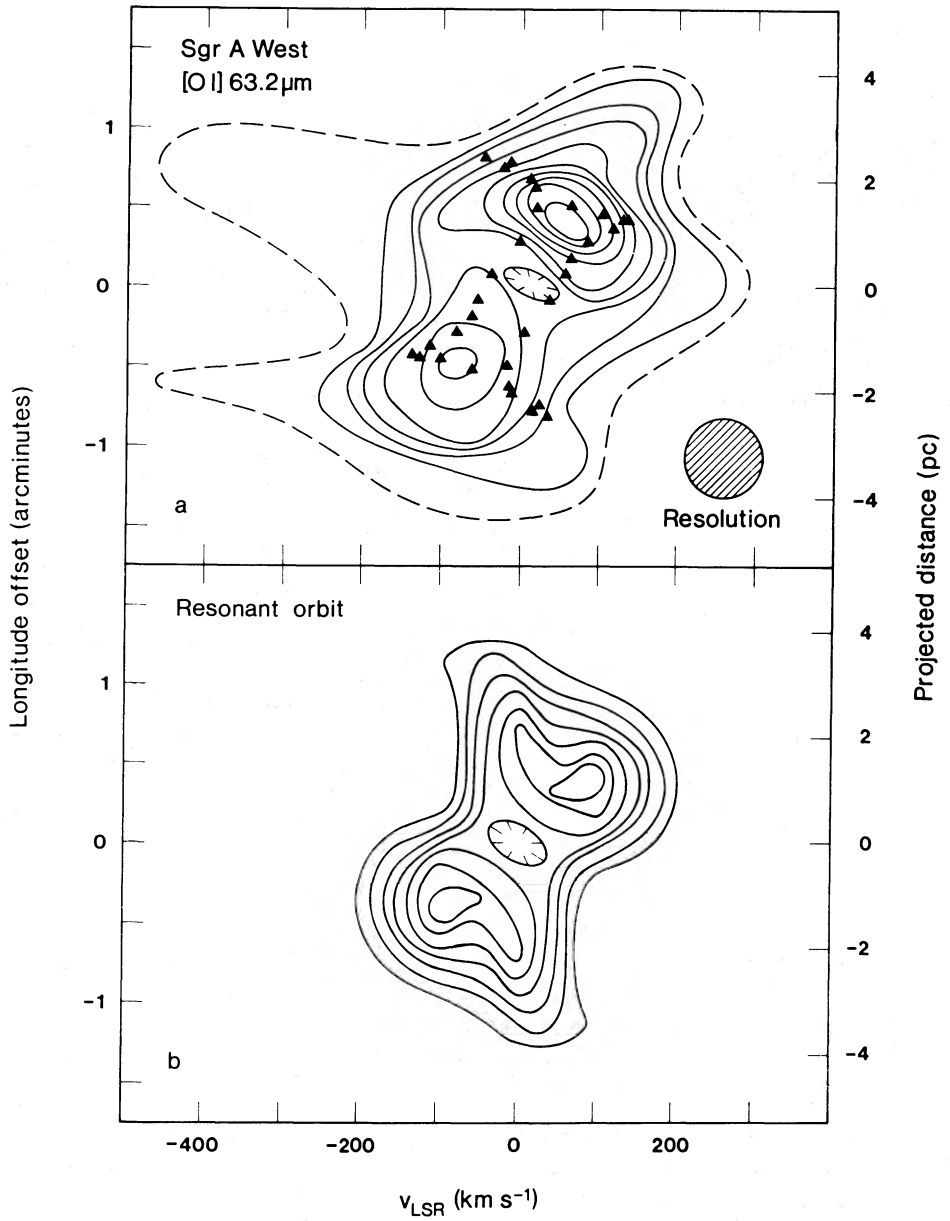

FIG. 13.—(*a*) The resonant orbit (*triangles*) superposed on the [O I] 63.2 μm longitude-velocity relation. The parameters used in the calculation were rotational velocity = 100 km s^{-1}, radial velocity amplitude = 85 km s^{-1}, pattern speed = 14.6 km s^{-1} pc^{-1} (angular velocity of the bar). The major axis of the orbit is perpendicular to the line of sight. (*b*) [O I] 63.2 μm emission from a uniform thin ring occupying the above orbit, convolved with the instrumental profile.

dissociated gas at the inner, exposed surfaces of individual cloudlets, while most of the interiors remain molecular. As the UV flux is gradually attenuated with increasing depth into the cloud, the fraction of photodissociated atomic and warm molecular material decreases. The dominant heating source of the atomic gas in the neutral disk is most likely the nonionizing UV (912–3000 Å) radiation from the center. Shock heating by cloud-cloud collisions may be important for the molecular gas.

The effects of tidal stripping plus frictional forces as well as cloud-cloud collisions probably cause material from the disk to fall into the center, while infall from clouds farther out or dynamical resonances of the gas in a slightly barred potential drive material into the disk.

The neutral disk rotates around the Galactic center. The rotation axis is remarkably similar to that of the Galactic rotation at much larger scales. The [O I] rotational velocity at 2 pc, the inner edge, corresponds to an enclosed mass of $(4.8 \pm 1) \times 10^6\ M_\odot$, and $(6.5 \pm 2.4) \times 10^6\ M_\odot$ is enclosed within 4.5 pc. If the innermost [Ne II] emission clouds in the bar observed by Lacy *et al.* (1980) are also primarily in circular motion, the mass enclosed within 0.2 pc is $(4.5 \pm 0.8) \times 10^6\ M_\odot$, and $(2.7 \pm 0.7) \times 10^6\ M_\odot$ is within 0.55 pc. In this case, most of the mass contained in 2 pc has to be contained in a region of <0.4 pc in diameter. The most likely form of such a mass concentration is a central point mass, such as a black hole. The data do not require a central point mass if the [Ne II] velocities are due to infall and the innermost ionized clouds have fallen in from a distance much larger than their current distance to the center, or if their motions are due to expansion from the center.

We are very grateful to the staff of the Kuiper Airborne Observatory for their excellent support and to the staff of the Richmond RAAF base, the Anglo-Australian Observatory, and the Institute for Astronomy, University of Hawaii, for their hospitality and help during our observations. We also thank J. Storey, M. Werner, H. Dinerstein, and D. Lester for help with the observing and instrument preparation, and J. Lacy, K. Y. Lo, and E. Serabyn for access to data prior to publication and for helpful discussions. This work was supported by NASA grant NAG-253.

APPENDIX

OH EXCITATION AND ABUNDANCE

I. COLLISIONAL EXCITATION

The upper level of the observed transition ($^2\Pi_{1/2}$, $J = 3/2 \rightarrow 1/2$) is the first excited rotational state in the $^2\Pi_{1/2}$ level. Collisional excitation of this level can proceed from the ground state ($^2\Pi_{3/2}$, $J = 3/2$) directly or via an intermediary excitation to the $^2\Pi_{1/2}$, $J = 1/2$ level. At high densities ($n > 10^7$ cm^{-3}) and temperatures ($T > 500$ K), the paths through the $^2\Pi_{3/2}$, $J = 5/2$ and the $^2\Pi_{1/2}$, $J = 5/2$ levels also contribute. We have computed level populations of the 12 lowest OH levels in the $^2\Pi_{1/2}$ and $^2\Pi_{3/2}$ ladders, assuming statistical equilibrium. Dewangan and Flower (1983) have calculated collision cross sections for the lowest six of these levels at a temperature of 280 K. To extend the calculations to all 12 levels and to both lower and higher temperatures, we have used cross sections published earlier for a range of temperatures (Dewangan and Flower 1982). These earlier calculations did not take into account spin-orbit coupling. To estimate all the necessary cross sections, including the effect of spin-orbit coupling, we scaled the 1982 cross sections at all temperatures by factors estimated from a comparison between the 1982 and 1983 values at 280 K. This is probably the best procedure until a larger set of cross sections becomes available. In accounting for radiative transport, an escape probability has been used, assuming a large velocity gradient and plane-parallel geometry. In this geometry the escape probability β is given by $\beta(\tau) = (1 - e^{-3\tau})/3\tau$. The large line widths in the Galactic center justify this approach. The uncertainties in the cross sections make the estimates uncertain by at least a factor of 2 in each direction. The observed intensity of each of the two $^2\Pi_{1/2}$, $J = 3/2 \rightarrow 1/2$ lines is $I_{OH} = (1.3 \pm 0.5) \times 10^{-4}$ ergs s^{-1} cm^{-2} sr^{-1}. To compute the density n_{H_2}, temperature T, and OH abundance χ_{OH} (relative to molecular hydrogen) necessary to account for this value, we adopt the total beam-averaged column density of hydrogen molecules estimated above ($N_{H_2} \approx 2 \times 10^{22}$ cm^{-2}). The volume filling factor Φ_v of the OH emitting gas is then

$$\Phi_v = 0.032\left(\frac{N_{H_2}}{2 \times 10^{22}\ \mathrm{cm}^{-2}}\right)\left(\frac{10^5\ \mathrm{cm}^{-3}}{n_{H_2}}\right)\left(\frac{6 \times 10^{18}\ \mathrm{cm}}{2R}\right), \tag{A1}$$

where R is the radius of the emission region. Since $\Phi_v \ll 1$ but $2R \gtrsim$ beam size, we in effect assume that the OH emission comes from a number of small clumps of radius R_c with a total beam filling factor $\Phi_A \approx \Phi_v(R/R_c)$. The observed line intensity then is given by

$$I_{OH} = \frac{2h\nu^4}{c^3}\frac{1}{n_l g_u/g_l n_u - 1}\Delta v \Phi_v^{2/3}[1 - \beta(\tau_{163})]\ . \tag{A2}$$

Here $\nu = 1.8 \times 10^{12}$ Hz, and n_l, n_u, and g_l, g_u are the populations and statistical weights of the $J = 1/2$ and $J = 3/2$ levels in the $^2\Pi_{1/2}$ ladder, respectively. The velocity width is $\Delta v \sim 100$–150 km s^{-1}, and $\beta(\tau_{163})$ is the escape probability for the 163 μm line (for an assumed velocity gradient of ~ 50 km s^{-1} pc^{-1}). This leads to a condition for the OH volume and column densities and OH abundance as a function of density and temperature required to match the observed line intensity.

Between $n_{H_2} \approx 10^5$–10^7 cm^{-3} and $200 \leq T \leq 600$ K, a good analytic approximation for the OH abundance in the Galactic center is

$$\chi_{OH} = \frac{N_{OH}}{N_{H_2}} = 10^{-5.3 \pm 0.5}\left(\frac{10^{7.5}\ \mathrm{cm}^{-3}\ \mathrm{K}}{n_{H_2} T}\right)\left(\frac{2 \times 10^{22}\ \mathrm{cm}^{-2}}{N_{H_2}}\right)^{2/3}\left(\frac{10^5\ \mathrm{cm}^{-3}}{n_{H_2}}\right)^{1/3}. \tag{A3}$$

As in the cases of the atomic gas and CO densities and temperatures must be fairly high to account for the far-infrared OH line emission assuming collisional excitation. This is a result of the high critical densities of the excited rotational states of OH ($n_{crit}^{OH} \sim 10^{10}$ cm^{-3}) and the low volume filling factor of the emission. In the likely regime of densities and temperatures the 163 μm OH optical depths are moderately high ($\tau_{163} \sim 0.5$–10), and trapping may significantly contribute to the line excitation.

In conclusion, if the OH $^2\Pi_{1/2}$, $J = 3/2$ state is collisionally excited in a gas component under conditions similar to those of the atomic gas ($n_{H_2} T = 10^{7.5}$ cm^{-3} K, $n_{H_2} = 10^5$ cm^{-3}), the OH column density is $\sim 10^{17}$ cm^{-2}. This corresponds to an OH abundance of $\sim 5 \times 10^{-6}$. As in the case of the CO emission, the required OH column density and OH abundance are less if the 163 μm line emission comes from dense (10^6 cm^{-3}), shock-excited gas ($n_{H_2} T \sim 10^9$ cm^{-3} K, $N_{OH} \sim 1.5 \times 10^{15}$ cm^{-2}, $\chi_{OH} \sim 10^{-7}$).

II. RADIATIVE EXCITATION

Radiative excitation of the $^2\Pi_{1/2}$, $J = 3/2 \rightarrow 1/2$ line may proceed by 54 and 35 μm pumping from the ground state to the $J = 3/2$ and 5/2 states in the $^2\Pi_{1/2}$ ladder. This mechanism appears promising, since the far-infrared continuum source in the Galactic center has a high color temperature, has peak flux between 30 and 50 μm, and is located within the OH source. For this pumping mechanism to work, $W_{cont}(\nu_{pump})$, the number of continuum photons emitted per second in the pump transitions [$^2\Pi_{3/2}$,

$J = 3/2 \rightarrow {}^2\Pi_{1/2}$, $J = 3/2$ (54 μm), ${}^2\Pi_{3/2}$, $J = 3/2 \rightarrow {}^2\Pi_{1/2}$, $J = 5/2$ (35 μm)] has to *exceed* W_{OH}, the total number of line photons emitted per second in the 163 μm transition:

$$W_{cont}(\nu_{pump}) = S_{cont}(\nu_{pump})\left(\frac{\Delta v 4\pi D^2}{hc}\right)$$

$$\geq W_{OH} = \frac{I_{OH}\Omega_{OH}}{h\nu_{OH}} 4\pi D^2 . \quad \text{(A4)}$$

Here Δv ($\sim$100–150 km s^{-1}) is the equivalent width of the OH lines, $\Omega_{OH} \sim 10^{-7}$ sr is the solid angle of the beam, and $D = 10$ kpc. The continuum flux densities by Rieke, Telesco, and Harper (1978), Gatley *et al.* (1978), and BGW correspond to $W_{cont}(54\ \mu m) \sim 6 \times 10^{49}$ s^{-1} and $W_{cont}(35\ \mu m) \sim 3 \times 10^{49}$ s^{-1}. The observed 163 μm OH intensity at $\Delta l = -40''$ corresponds to $W_{OH} \sim 1.5 \times 10^{49}$ s^{-1}. Thus, infrared pumping is possible. Furthermore, a large fraction of the 35 and 53 μm continuum photons must be *absorbed* by OH molecules surrounding the continuum source. Assuming that the OH region covers a large enough solid angle, the pump transitions also have to be optically thick [$\tau_{OH}(35\ \mu m), \tau_{OH}(54\ \mu m) \gtrsim 1$]:

$$1 \leq \tau_{OH} \sim 3 \times 10^{13} g_u A_{u0} E_{u0}^{-3} \chi_{OH} . \quad \text{(A5)}$$

Here $g_u = 2J_u + 1$ is the statistical weight of the upper level of the pump transition, A_{u0} is the Einstein coefficient, and E_{u0} is the energy difference between the upper level and the ground state, in K. The OH abundance has to be $\geq 2 \times 10^{-6}$ for $\tau(54\ \mu m) \geq 1$ and $\geq 1.2 \times 10^{-5}$ for $\tau(35\ \mu m) \geq 1$. This estimate is confirmed by a more complete numerical calculation with the observed continuum fluxes as input parameters for a background continuum field. The OH abundance has to be $\geq 10^{-6}$ if the OH cloud completely covers the outside of the continuum source. We conclude that the observed 163 μm emission requires a high abundance of OH ($\chi_{OH} = 10^{-7}$–10^{-5}) in the Galactic center, independent of excitation mechanism.

Such a high OH abundance may indicate that shock chemistry (Hartquist, Oppenheimer, and Dalgarno 1980), or UV photochemistry, is more important that ion-molecule chemistry in this region. The double-ladder structure of the OH molecule allows unambiguous determination of the excitation mechanism by comparison of excited transitions in the ${}^2\Pi_{1/2}$ ladder to those in the ${}^2\Pi_{3/2}$ ladder. While a number of the excited states of the ${}^2\Pi_{1/2}$ ladder can be directly populated by radiative excitation from the ground state as well as by collisional excitation, the excited states of the ${}^2\Pi_{3/2}$ ladder can be populated only by collisions. Here we have not counted sequential pumping from one level to the next in a given ladder, since that does not lead to emission lines. In the case of collisional excitation with the parameters given above, the 84 μm ${}^2\Pi_{3/2}$, $J = 7/2 \rightarrow 5/2$ line, for example, should be about an order of magnitude more intense than the 163 μm ${}^2\Pi_{1/2}$, $J = 3/2 \rightarrow 1/2$ line. For the case of radiative excitation, no 84 μm emission or absorption would be present. A preliminary measurement of the 84 μm spectra in a 30″ beam toward the center position resulted in an upper limit of 2×10^{-3} ergs s^{-1} cm^{-2} sr^{-1}, thus marginally favoring radiative excitation of OH in Agr A.

REFERENCES

Becklin, E. E., Gatley, I., and Werner, M. W. 1982, *Ap. J.*, **258**, 135 (BGW).
Beckwith, S., Persson, S. E., Neugebauer, G., and Becklin, E. E. 1978, *Ap. J.*, **223**, 464.
Bieging, J. H. 1976, *Astr. Ap.*, **51**, 289.
Bohlin, R. C., Savage, B. D., and Drake, J. F. 1978, *Ap. J.*, **224**, 132.
Brown, J. M., Schubert, J. E., Evenson, K. M., and Radford, H. E. 1982, *Ap. J.*, **258**, 899.
Brown, R. L., Johnston, K. J., and Lo, K. Y. 1981, *Ap. J.*, **250**, 155.
Brown, R. L., and Liszt, 1984, *Ann. Rev. Astr. Ap.*, **22**, 223.
Burton, W. B., and Liszt, H. S. 1978, *Ap. J.*, **225**, 815.
Combes, F., and Gerin, M. 1984, *Astr. Ap.*, submitted.
Crawford, M. K., Genzel, R., Townes, C. H., and Watson, D. M. 1985, *Ap. J.*, **291**, 755.
Davies, P. B., Handy, B. J., Murray Lloyd, E. K., and Smith, D. R. 1978, *J. Chem. Phys.*, **68**, 1135.
Dewangan, D. P., and Flower, D. R. 1982, *M.N.R.A.S.*, **199**, 457.
———. 1983, *J. Phys. B.*, **16**, 2157.
Ekers, R. D., van Gorkom, J. H., Schwarz, U. J., and Goss, W. 1983, *Astr. Ap.*, **122**, 143.
Ellis, B., and Werner, M. W. 1985, in preparation.
Freeman, K. C. 1970, *IAU Symposium 38, The Spiral Structure of Our Galaxy*, ed. W. Becker and G. Contopoulos (Dordrecht: Reidel), p. 351.
Gatley, I. 1983, in *Galactic and Extragalactic Infrared Spectroscopy*, ed. M. F. Kessler and J. P. Phillips (Dordrecht: Reidel).
Gatley, I., Becklin, E. E., Werner, M. W., and Harper, D. A. 1978, *Ap. J.*, **220**, 822.
Gatley, I., Jones, T. J., Hyland, A. R., Beattie, D. H., and Lee, T. J. 1984, *M.N.R.A.S.*, **210**, 565.
Gautier, T. N. 1979, Ph.D. thesis, Umiversity of Arizona.
Geballe, T. R., Krisciunas, K., Lee, T. J., Gatley, I., Wade, R., Duncan, W. D., Garden, R., and Becklin, E. E. 1984, *Ap. J.*, **284**, 118.
Genzel, R., Watson, D. M., Townes, C. H., Dinerstein, H. L., Hollenbach, D., Lester, D. F., Werner, M., and Storey, J. W. V. 1984, *Ap. J.*, **276**, 551 (Paper I).
Güsten, R., and Downes, D. 1980, *Astr. Ap.*, **87**, 6.
Hall, D. N. B., Kleinmann, S. G., and Scoville, N. Z. 1982, *Ap. J. (Letters)*, **262**, L53.
Hartquist, T. W., Oppenheimer, M., and Dalgarno, A. 1980, *Ap. J.*, **236**, 182.
Herter, T., Houck, J. R., Shure, M., Gull, G. E., and Graf, P. 1984, *Ap. J. (Letters)*, **287**, L15.
Hildebrand, R. H. 1983, *Quart. J. R.A.S.*, **24**, 267.
Ho, P. T. P., Jackson, J. M., Barrett, A. H., and Armstrong, J. 1985, *Ap. J.*, **288**, 575.
Hohl, F. 1971, *Ap. J.*, **168**, 343.
Inguscio, M., Evenson, K. M., Beltrán-López, V., and Ley-Koo, E. 1984, *Ap. J. (Letters)*, **278**, L127.
Lacy, J. H., Townes, C. H., Geballe, T. R., and Hollenbach, D. J. 1980, *Ap. J.*, **241**, 132.
Lacy, J. H., Townes, C. H., and Hollenbach, D. J. 1982, *Ap. J.*, **262**, 120.
Launay, J. M., and Roueff, E. 1977*a*, *Astr. Ap.*, **56**, 289.
———. 1977*b*, *J. Phys. B.*, **10**, 879.
Lester, D. F., Werner, M. W., Storey, J. W. V., Watson, D. M., and Townes, C. H. 1981, *Ap. J. (Letters)*, **248**, L109.
Liszt, H. S., and Burton, W. B. 1980, *Ap. J.*, **236**, 779.
Liszt, H. S., Burton, W. B., and van de Hulst, J. M. 1984, preprint.
Liszt, H. S., van de Hulst, J. M., Burton, W. B., and Ondrechen, M. P. 1983, *Astr. Ap.*, **126**, 341.
Lo, K. Y., and Claussen, M. J. 1983, *Nature*, **306**, 647.
McKee, C. F., Storey, J. W. V., Watson, D. M., and Green, S. 1982, *Ap. J.*, **259**, 647.
Novak, G., *et al.* 1985, in preparation.
Prasad, S. S., and Huntress, W. T., Jr. 1980, *Ap. J. (Suppl.)*, **43**, 1.
Quinn, P. J., and Sussman, G. J. 1985, *Ap. J.*, **288**, 377.
Rieke, G. H., Telesco, C. M., and Harper, D. A. 1978, *Ap. J.*, **220**, 556.
Schwarz, M. P. 1981, *Ap. J.*, **247**, 77.
Serabyn, E. 1984, Ph.D. thesis, University of California, Berkeley.
Serabyn, E., and Lacy, J. H. 1985, in preparation.
Shull, J. M., and McKee, C. F. 1979, *Ap. J.*, **227**, 131.
Stacey, G., Kurtz, N., Smyers, S., Harwit, M., Russell, R., and Melnick, G. 1982, *Ap. J.*, **257**, L37.
Storey, J. W. V., and Allen, D. A. 1983, *M.N.R.A.S.*, **204**, 1153.
Storey, J. W. V., Watson, D. M., and Townes, C. H. 1980, *Internat. J. Infrared Millimeter Waves*, **1**, 15.
———. 1981, *Ap. J. (Letters)*, **244**, L27.
Storey, J. W. V., Watson, D. M., Townes, C. H., Haller, E. E., and Hansen, W. L. 1981, *Ap. J.*, **247**, 136.

Tielens, A., and Hollenbach, D. J. 1984*a*, *Ap. J.*, **291**, 722.
———. 1984*b*, *Ap. J.*, **291**, 747.
van Gorkom, J. H., Schwarz, U. J., and Bregman, J. D. 1984, in *IAU Symposium 106, The Milky Way Galaxy*, ed. H. van Woerden, W. B. Burton, and K. J. Allen (Dordrecht: Reidel).
Watson, D. M. 1982, Ph.D. thesis, University of California, Berkeley.
———. 1984, in *Galactic and Extragalactic Infrared Spectroscopy*, ed. M. F. Kessler and J. P. Phillips (Dordrecht: Reidel), p. 195.
Watson, D. M., Crawford, M. K., Genzel, R., and Townes, C. H. 1985*a*, in preparation.
Watson, D. M., Genzel, R., Townes, C. H., and Storey, J. W. V. 1985*b*, *Ap. J.*, forthcoming.
Watson, D. M., Storey, J. W. V., Townes, C. H., and Haller, E. E. 1980, *Ap. J. (Letters)*, **241**, L43.
Whitcomb, S. E., Gatley, I., Hildebrand, R. H., Keene, J., Sellgren, K., and Werner, M. W. 1981, *Ap. J.*, **246**, 416.
Young, J. S., and Scoville, N. Z. 1982, *Ap. J.*, **258**, 467.

M. K. CRAWFORD: DuPont Experimental Station, Room 217, Building 356, CR&D, Wilmington, DE 19898

R. GENZEL and C. H. TOWNES: Department of Physics, University of California, Berkeley, CA 94720

DAN M. WATSON: Department of Physics, 320-47, California Institute of Technology, Pasadena, CA 91125